JOINT EUROPEAN TORUS JET

JET–P(92)77

J. Jacquinot, V.P. Bhatnagar, C. Gormezano
and JET Team

JET Recent Results on Wave Heating and Current Drive; Consequences for Future Devices

JET Recent Results on Wave Heating and Current Drive; Consequences for Future Devices

J. Jacquinot, V.P. Bhatnagar, C. Gormezano and JET Team*

JET-Joint Undertaking, Culham Science Centre, OX14 3DB, Abingdon, UK

** See Annex*

Preprint of Paper to be submitted for publication in
Plasma Physics and Controlled Fusion

JET RECENT RESULTS ON WAVE HEATING AND CURRENT DRIVE CONSEQUENCES FOR FUTURE DEVICES

J Jacquinot, V P Bhatnagar, C Gormezano and the JET Team

JET Joint Undertaking, Abingdon, Oxon, OX14 3EA

ABSTRACT

The latest developments of the JET ICRH and LHCD systems are reviewed. Feedback controls have alleviated the traditional difficulties with plasma-antenna coupling. Experimental results on high plasma performance, basic confinement aspects and issues relevant to the next generation of tokamaks are described. ICRH allows a narrow power deposition profile to be localised at will independently of the plasma density and size. We demonstrate that in large tokamaks, the constraint to use a minority species can be removed and heating a balanced D/T mixture at $\omega = \omega_{CD}$ in ITER is proposed. LHCD allows the highest current drive efficiency to be obtained. The conditions for wave accessibility are discussed in light of the JET results. LHCD is well adapted to save volt seconds in the current rise phase. The observed synergistic LHCD/ICRH acceleration of fast electrons is a promising route towards higher current drive efficiency but raises unresolved physics aspects which are analysed. We finally consider the prospects of a steady state fusion reactor.

KEYWORDS

Tokamak, Heating, Current drive, ICRH, LHCD, FWCD, Confinement, H-modes, Fusion Yield, Bootstrap Current, ITER, Steady State Fusion Reactors.

1. INTRODUCTION

JET has successfully developed 3 high power auxiliary systems (Rebut et al, 1990; Keilhacker, 1992) based on (a) Neutral Beam Injectors (NBI) at 70 to 140 keV, (b) Radio Frequency waves (23 to 57 MHz), hereafter referred to as Fast Waves or Ion Cyclotron Resonance Heating (ICRH) and (c) Lower Hybrid waves (3.7 GHz) called LHCD for Lower Hybrid Current Drive. The first 2 systems have allowed to assemble a significant data base on plasma heating and confinement to combined powers of up to 35 MW. The 2 different heating techniques have been to a large extent complementary by extending the plasma operational space and also by revealing basic aspects of plasma confinement which are universal, being independent of the heating method which was used. The third method (LHCD) is aimed at the control of the plasma current profile by driving a significant part of the plasma current either alone or in combination with current drive capabilities of the other 2 methods.

The results obtained in JET and in other tokamaks have given the impetus to launch a design of a larger device aiming at long pulse ignition called ITER (Tomabeshi, 1990) which is presently entering the Engineering Design Activity phase. It is therefore an appropriate time to review the results and make the necessary extrapolation to a larger plasma size and for the parameters foreseen in a fusion reactor (Rebut, 1992). The review and the extrapolation of the experimental results obtained with the 2 JET high power wave systems is the subject of this article. The material for the review has been drawn from contributions to this topical conference, from contributions to the EPS conference of the Plasma Physics Division held the previous week in Innsbruck and finally from 2 previous summary articles (Jacquinot et al, 1991 and 1992). The reader is referred to these 2 articles for an introduction to the wave physics aspects which form the basis of the 2 RF methods. The paper is organised as follows:

The technical aspects of the systems are described with the emphasis placed on the operating domains and original aspects of the specifications. The second chapter is an overview of confinement and performance studies performed with these RF systems used as "standard tools" during scientific programmes aimed at general topics. They illustrate the versatility and limitations of the methods. We then describe experiments dedicated to specific RF physics aspects and whenever possible extrapolate the results to ITER plasmas. The new experiments on high minority concentration and current drive regimes fall into this category. The conclusions give the authors views on the most attractive applications of RF systems for ITER.

2. THE JET ICRH AND LHCD SYSTEMS

2.1 ICRH (Fast Wave)

The upper limit of the frequency range (57 MHz) of the ICRH system is determined by the proton cyclotron resonance for the maximum magnetic field (3.4 T) on the axis. The lower limit (23 MHz) is set by the requirement to work at the deuterium cyclotron resonance during the D/T phase of JET. The amplifiers of each generator module can be set remotely to any frequency in the band except between 39 and 41 MHz where spurious resonances of the amplifier circuit have been parked.

The dynamic bandwidth at each frequency is ±2 MHz. The control systems are highly automated so that the plant can be operated as a standard tool by non-specialists. The automation includes: the possibility to change operating frequency in about one minute and feedback loops which are listed in Table 1.

Table 1: Characteristics of the ICRF Plant

Frequency Range	• 23 to 57 MHz for D, ^{3}He or H cyclotron resonance on axis
8 Generator modules	• 4 MW (20 s) output per module using 2 tetrode amplifiers
8 Antennae	• Screen made of beryllium bars (15° inclination)
(only 7 used in this work)	• 2 adjacent loops operated with either Monopole phasing (0,0) or dipole phasing (0,π), or arbitrary phase
	• Getter pumps on vacuum transmission lines
16 Transmission lines (Generator to antenna)	• Each line 84 m long rated at 50 kV peak (ϕ ~ 230 mm, 30 ohms)
Feedback loops for	• Plasma position for constant coupling resistance
	• RF power level or antenna RF current
	• Phase between the antennae
	• Frequency (Δν ~ 1 MHz) for matching
	• Motorised tuning stub for matching
	• Tetrode screen dissipation (acting on anode voltage)
Maximum coupled power	• 22 MW

These loops have different response times ranging from 1 ms for the loop acting on frequency to 0.5 s for mechanical displacement of the tuning stub. The more recent developments include a loop acting on the plasma horizontal position which maintains constant the coupling resistance and a feedback (Bosia, Jacquinot, 1991) which provides antenna matching for a prescribed phase difference and current in the 2 antenna straps. These new additions have been essential elements in current drive experiments and in all situations where the plasma at the boundary changes substantially during the heating phase. A particular striking use of the feedback facilities was evident during the high bootstrap current experiments (section 3.2) when the plasma went in sequence from L-mode to an elmy H-mode then to an elm-free H-mode with progressive increase of β_p to 2 creating a substantial triangular deformation of the plasma equilibrium. The antenna coupling resistance was maintained at 3 ohms by the feedback loops during the entire process (Fig 1). A diagram of the ICRH system can be seen in Fig 2.

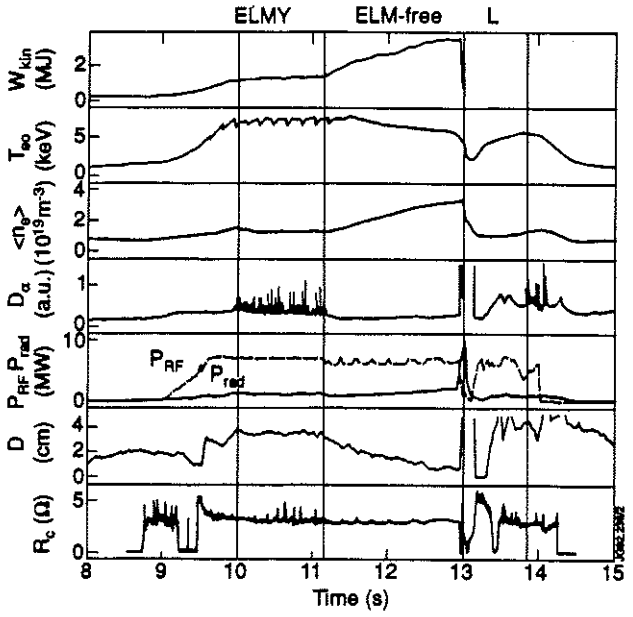

Fig 1. Main plasma quantities during a high bootstrap current discharge I_p = 1 MA. The plasma position feedback system maintains the coupling resistance (R_c) constant despite large variations of the plasma shape in the various confinement phases.

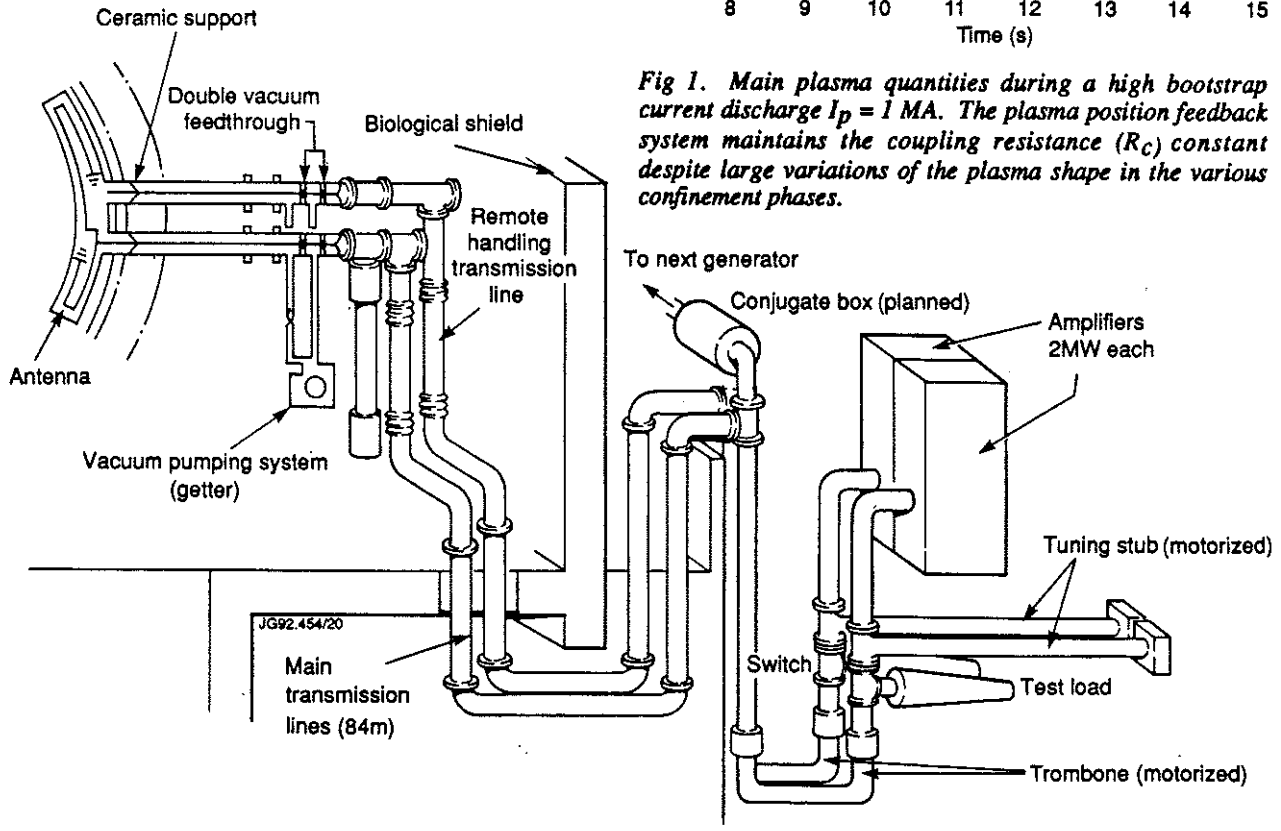

Fig 2. Schematic diagram of one module of the JET ICRH system.

Three generations of JET ICRH antennae have been tested during the last 10 years evolving from a single strap loop antenna with horizontal nickel screen bars to a multi-strap design with beryllium screen-bars with an inclination matching approximately the direction of the tokamak magnetic field (Kaye, 1992). The new design reduces, to negligible levels, the impurity release specific to ICRH (Bures et al, 1991) although edge convective cells (Jacquinot, D'Ippolito et al, 1991) are still expected when the following 2 conditions are met simultaneously: insufficient alignment of the screen bars and phasing between adjacent straps departing from π. Such convective cells may affect plasma confinement near the outer edge. Figs 3a and 3b show the ICRH antenna and the lower hybrid launcher as installed in the JET vessel during the 1991 - 1992 experimental campaign.

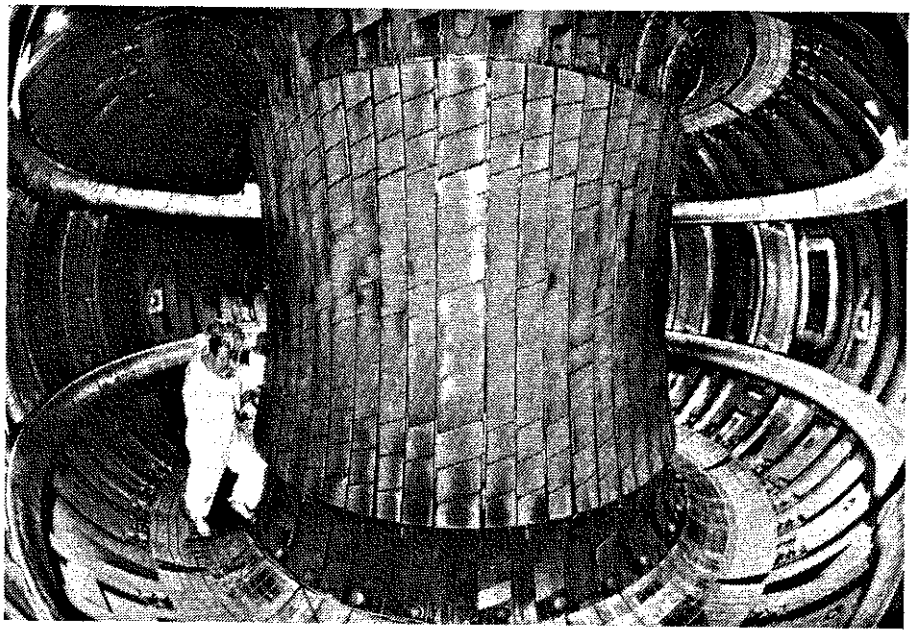

Fig 3a. Interior of the JET vessel showing the belt limiters, 4 ICRH antennae, the LHCD launcher (right) and the inner wall.

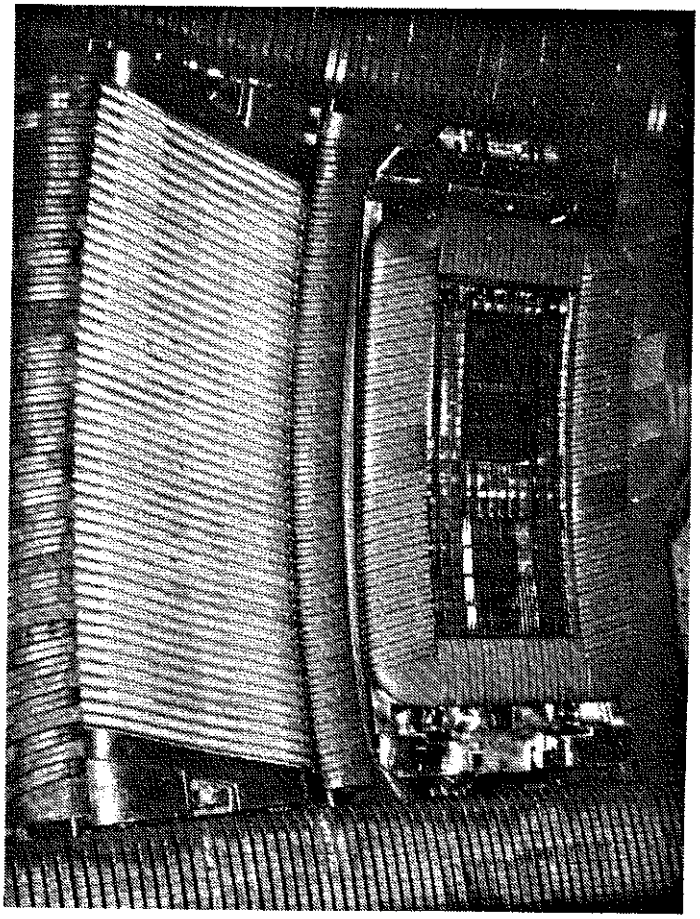

Fig 3b. Close-up on the ICRH antenna (beryllium tilted screen) and on the LHCD launcher.

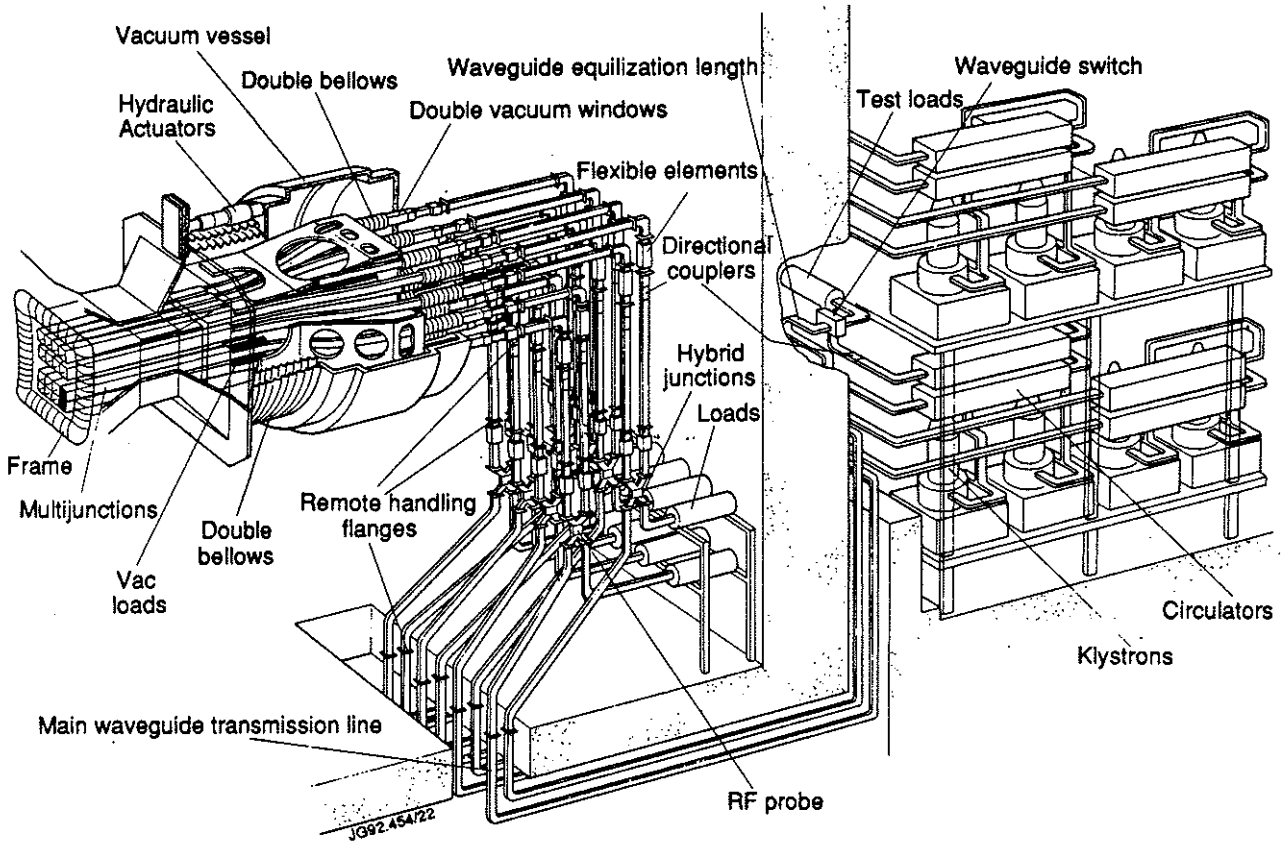

Fig 4. Schematic diagram of the JET LHCD system.

2.2 LHCD (Slow Wave)

The frequency of the lower hybrid system has been fixed to 3.7 GHz. This choice takes advantage of technical developments made in Tore Supra (Tonon et al, 1991) while being sufficiently high to avoid wave coupling to fast ions and to allow wave penetration to the plasma core up to $n_e \sim 3\ 10^{19}\ m^{-3}$ (see section 4.3). The characteristics of the prototype system (Gormezano et al, 1987) used in the experiments reported here are given in Table 2 and a sketch of its main components is shown in Fig 4. The power generated by each klystron is split via 2 hybrid junctions and a multijunction into 16 waveguides at the grill mouth. The generation of a well-defined wave spectrum with a high directivity is essential for current drive application and particular emphasis has been placed in controlling the wave phase in each waveguide. An accuracy of 10° is obtained by a tight control of the mechanical dimensions of the splitting network and by feedback control of the phase at the output of each klystron.

Table 2: LHCD Parameters

Generator	**Prototype System** ***(full system in brackets)***
Frequency	3.7 GHz
Number of klystrons	8, (24)
Power (generator)	
10s pulse	4.8 MW
20s pulse	4 MW (12 MW)
Duty cycle	1/30
Efficiency	42 %
Phase control	10 degrees accuracy
Maximum VSWR	1.8
Length of transmission line	40 m
Estimated insertion losses	1 dB
Launcher	
Number of waveguides	128, (384)
Waveguide material	stainless steel and ZiCo (stainless steel)
Coating	copper + carbon, (copper)
Maximum temperature	350° C
Total weight	12 tons, (15)
Stroke	210 mm
Response	12 mm/15 ms
Maximum coupled power	2.7 MW

The entire launcher structure (10 tons) can be moved during plasma operation by 21 cm using hydraulic actuators. The launcher movement can be either programmed or controlled by a feedback loop maintaining the standing wave ratio in the waveguides at a requested value. Such a feedback system was used during the current rise of high performance discharge at 7 MA (Fig 5, to be discussed also in Section 3.3) in order to compensate for significant changes of the plasma shape during this transient phase. JET is now considering implementing another feedback loop on the plasma horizontal position to maintain the average reflectivity constant . The new system will have the advantage of a faster time response (30 ms) than the hydraulic actuators.

2.3 Operating Domains

Both the fast waves generated by ICRH antennae and the slow waves excited by the LHCD launcher are evanescent between the coupling structure and a density contour where the waves start to propagate inwards. The tunnelling factor of the wave through this evanescent zone has to be large enough to prevent excessive reflection at the coupling structure. This condition is achieved for a small value of the distance D between the coupler and the last closed surface, for sufficient edge density n_{ea} and for large connection lengths $L_{||}$ of the magnetic field near the coupler. A relevant coupling parameter describing the density at the launcher is: $C_p = n_{ea}\, D/\sqrt{L_{||}}$. A dependence on $D/\sqrt{L_{||}}$ is observed experimentally (Ekedahl et al, 1992) in close agreement (Fig 6) with detailed coupling theory for both the slow wave and fast wave. In practice, high power experiments require D to be less than 3 cm for LHCD and less than 5 cm for ICRH. The higher values can be used for the large connection lengths ($L_{||} \geq 40$ m) which arise in X-point plasmas or for plasmas resting on the inner wall. The single null geometry foreseen for the future JET pumped divertor phase and for ITER is favourable providing large $L_{||}$ value ($\simeq$ 50 m) and 19 MW of ICRH has been coupled with 7 antennae in this geometry (D $\simeq$ 3 cm).

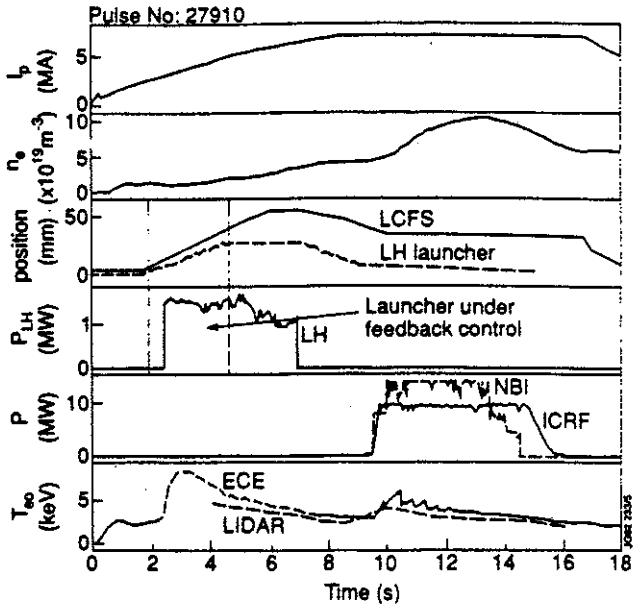

Fig 5. Combined operation of LHCD, ICRH and NBI during long 7 MA experiments (8.5 s). The 12 tons LHCD coupler is allowed to move by 30 mm under feedback control of the VSWR in the waveguide.

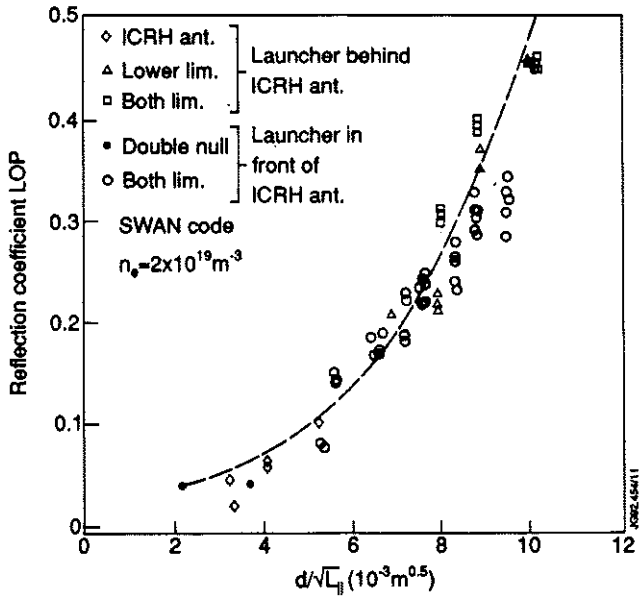

Fig 6. Reflection coefficient versus $DL_{//}^{-0.5}$ ($L_{//}$ is the connection length and D the distance between the coupler and the last closed surface. Comparison with the SWAN coupling code.

3. HIGH PERFORMANCE REGIMES AND CONFINEMENT STUDIES

We intend in this chapter to illustrate several modes of operations using the RF systems in order to achieve high performance regimes or to perform specific confinement studies. It will become apparent that the versatility of the systems was well employed: the operating regimes included limiter, double null or single null configurations, the density ranges from 10^{19} to 2 10^{20} m^{-3}, the toroidal field scans from 1.2 to 3.4 T and the pulse length extends to 60 s.

3.1 High Performance Regimes

3.1.1 High Fusion Reactivity

3.1.1.1 ICRH-dominated Scenarios. Resonant cyclotron acceleration of ^{3}He in a deuterium plasma has led to 140 kW for several seconds of D-^{3}He fusion power and to a maximum fusion amplification Q = 1.25 % (Jacquinot and Sadler, 1991): the fusion power scales linearly with the energy stored in the fast ions as expected from the quasi-linear theory of high energy tail development under resonant acceleration by RF. Such a regime has potential applications in advanced fuel fusion reactors; it is also a test of principles for the (D)T scenario proposed for JET and ITER. In both modes of operation the concentration $\eta = n_{min}/n_e$ of the resonating species needs to be controlled in order to achieve the tail energy corresponding to the optimum reactivity. In JET $\eta_{optimum}$ is between 0.05 to 0.1 in (^{3}He)D and is calculated to be between 0.2 to 0.3 in the (D)T case. The high concentration scenarios required in the later case have recently been demonstrated for the first time (see Chapter 4).

Central ICRH, after deep pellet injection, benefits from combined effects of improved central confinement, H-mode and a well localised heat deposition profile (Tubbing et al, 1991). A maximum fusion product of $n_D(O)\, \tau_E T_i(O) = 7.8\ 10^{20}$ m^{-3} s keV

is obtained which is one of the highest seen in JET. More recently, it has been possible to increase (albeit at low density) the central ion temperature up to 16 - 18 keV by operating at higher concentration and/or by using 2 frequencies and 2 resonating species (H and ^{3}He) in order to increase bulk ion heating by preventing the minority tail energy to extend far into the electron drag regime. An example of such a discharge is shown in Fig 7. The optimism generated by these results has been moderated by the fact that the duration of the high confinement phase could not be extended beyond 1.5 s due to MHD instabilities. The bootstrap current resulting from the large pressure gradient is thought to lead to shear reversal (Schmidt et al, 1989) which could be responsible for the good central confinement but, when excessive, would also lead to the large MHD instabilities (Hugon et al, 1992). Control of the current density by non-inductive current drive methods is suggested in order to prevent excessive shear reversal.

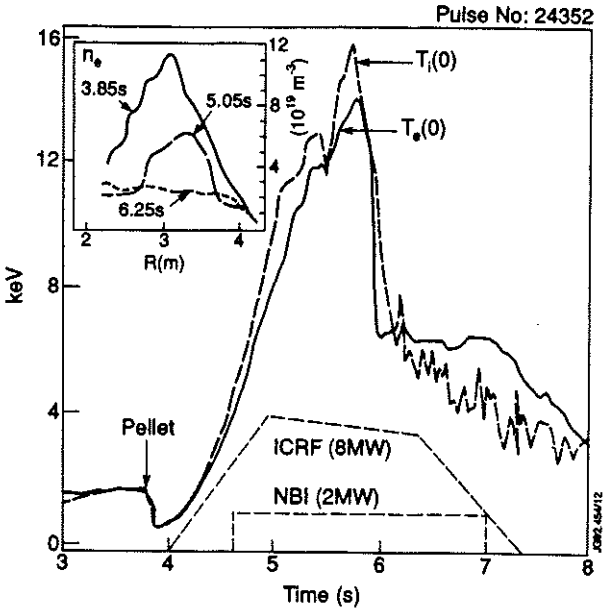

Fig 7. High performance with ICRH following deep pellet injection. High minority concentration leads to increased central ion temperature.

3.1.1.2 ICRH in NBI dominated hot ion modes.
Hot ion mode discharges on JET are produced by high power Neutral Beam Injection (NBI) into a low density plasma $< n_e > \simeq 1 \times 10^{19}$ m^{-3} in either double (DNX) or single (SNX) null X-point configurations. The central particle fuelling combined with mainly ion heating by NBI results in a discharge which, in addition to the H-mode enhancement, benefits from improved central confinement. The beam injection energy is 140 keV which corresponds to the maximum of the D/T fusion cross-section; the same energy also corresponds to central fuelling in JET-size plasmas. Adding ICRH power (1.5 to 6 MW, H minority) on these discharges with 15 MW NBI results in the following changes (Bures et al, 1992).

a) $\delta T_{eo} \simeq \delta T_{io} \simeq 1.5$ to 3 keV

b) $\delta(dR_{DD}/dt) \simeq 30$ to 50 % (R_{DD} is the D-D reaction rate)

c) an earlier appearance of the carbon bloom which prevents progress on the peak reactivity (Fig 8).

It is also found that NBI power can be exchanged for RF power at the level of a few MW whilst maintaining or even increasing the fusion reactivity. The increase of T_{eo} and T_{io} when projected to D-T mixtures will allow JET to achieve higher fusion power than with NBI only but Q is expected to decrease slightly unless additional favourable factors such as sawtooth stabilisation come into play. The observed increase of the D-D fusion reactivity is only partially relevant to D-T operation since part of it results from RF acceleration of Deuterium ions which reach too high an energy to make an effective contribution to the D-T reactivity. Calculations (Eriksson, 1992) based on the parameters achieved during the first Tritium Experiment suggest using for the next JET Tritium experiment about 4 MW of ICRH for accelerating deuterium beam ions at $\omega = \omega_{cd}$ supplemented by 2 MW of hydrogen minority heating as a complement to raise T_e and T_i. The effect would be to increase the fusion reactivity by 30 % with about 5 % decrease in Q. Using higher RF power levels would increase further the fusion power but the decrease in Q would be more substantial since Deuterium ions would be driven past the energy corresponding to the optimum fusion cross-section.

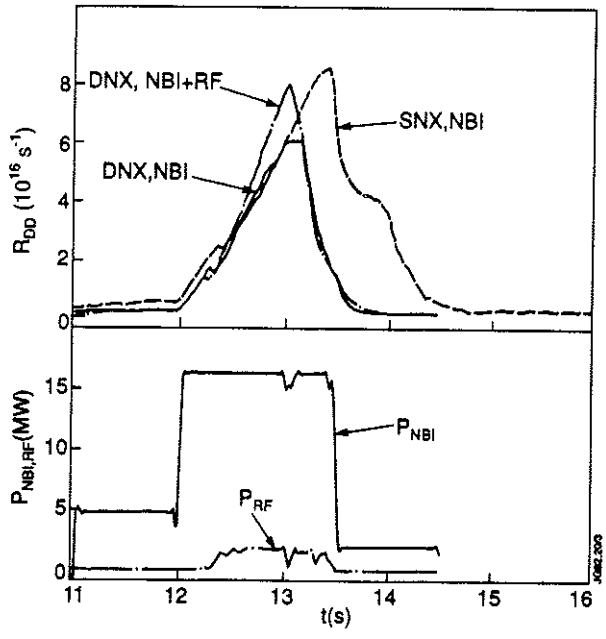

Fig 8. Fusion reaction rate in Deuterium plasmas during hot ion H-modes. Pure NBI heated discharges are compared to ICRH supplemented discharges. The NBI single null (SNX, NBI) and the combined heating double null (DNX, NBI + RF) are the discharges with the highest fusion yield in JET discharges recorded in each X-point configuration. Adding ICRF increases dR_{DD}/dt but the roll over occurs earlier.

3.2 Bootstrap Current Dominated ICRH Plasmas Combined with High Confinement

The prospects for a long burn tokamak reactor are improved if a substantial fraction of the plasma current can be driven by the neoclassical bootstrap effect. Previous experiments using neutral beam injection show that a significant fraction of the plasma current (up to 80 % in the JT-60 case) could be attributed to the bootstrap current. In JET, the effect was shown to be compatible with H-mode confinement. The experiments performed recently, with ICRH as the sole additional heating method (Challis et al, 1992), aimed at extending the high bootstrap regimes to conditions with negligible central particle fuelling and in the absence of neutral beam fast ion current.

Since the bootstrap current fraction can be written: $I_{BS}/I_p \sim \sqrt{a/R}\,\beta_p$, it is essential to reach high values of β_p, the plasma pressure normalised to poloidal field pressure. Heating double-null X-point discharges at low plasma current (I_p = 1 to 1.5 MA, 2.8 - 3.1 T) with 4 - 10 MW of ICRH resulted in $\beta_p \leq 2$ during the elm-free phase of the H-mode (Fig 1). Detailed comparison (Challis et al, 1992) of the surface loop voltage with values calculated by TRANSP infers a bootstrap current fraction of 35 % during the elmy phase rising to 70 % during the elm-free phase. In the experiment, the surface voltage remains negative during the entire 3 s pulse due to the d Li/dt term as the current channel is broadened by the large contribution of the bootstrap current.

The elm-free phase is terminated by a sudden event which can result in the loss of more than 50 % of the electron density and plasma energy (Fig 9). Edge ballooning modes possibly combined with antenna-plasma contact are plausible reasons for the event (Hender, 1992). It is remarkable that the elm-free H-mode is re-established almost immediately after the event resulting in a quasi-steady state relaxation process with the average β per cycle being almost 90 % of the peak value.

The thermal energy confinement time of these plasmas is up to 80 % better than the value given by the ITER H-mode scaling (Fig 10). It should be noted that the data was obtained with higher q values at the plasma edge but also in conditions closer to steady state compared with that used for the scaling.

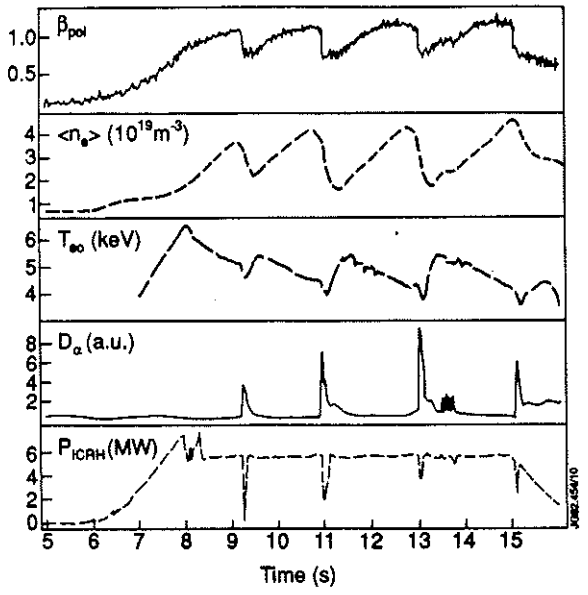

Fig 9: Large periodic relaxation of the elm-free phase of high bootstrap current, high normalised confinement discharges. Sawtoothing is small and limited to the beginning of each elm-free phase.

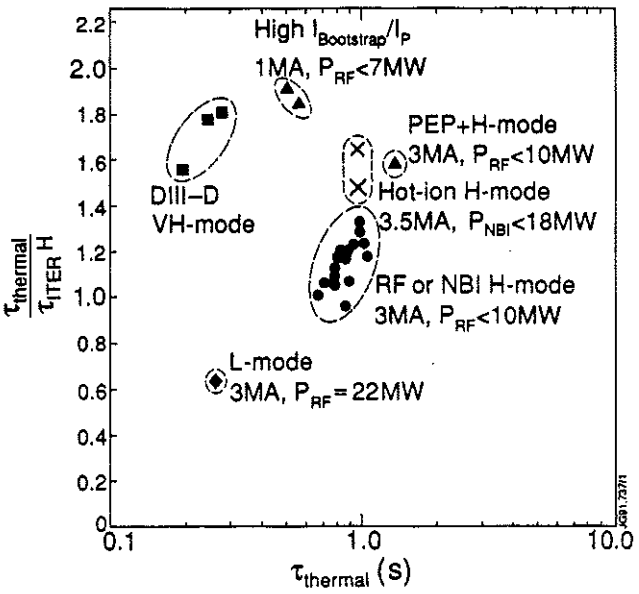

Fig 10: Summary of the JET modes of operation. The normalisation of the vertical axis refers to ITER H-mode scaling $\tau_{ITER}^{H} = 0.106\ P^{-0.46}\ I_p^{1.03}\ R^{1.48}$ which is approximately twice the L-mode Goldston scaling.

3.3 Long Pulses (up to 60 s), Operation at 7 MA and at High Density

Both the JET ICRH and LHCD launchers are not actively cooled. In fact, the RF power losses in these devices are quite small and the full pulse length specifications (20 s for ICRH and 50 s at reduced power for LHCD) have been achieved without significant heating effects on the launcher although it has been noted (Ekedahl et al, 1992) that the LHCD launcher becomes progressively deconditioned during a series of long pulses due to the lack of pumping within the launcher structure.

LHCD and ICRH have been prime instruments during long pulse research in JET since they provide substantial volt-second savings by increasing the bulk electron temperature and, in the case of LHCD, by generating current drive. A good illustration is given in Fig 11 where the combined application of ICRH and LHCD extended the duration of the basic ohmic discharge (2 MA) by 25 s. In this case the plasma termination is caused by the toroidal field system reaching its limiting I^2t value. These experiments gave information on the time scale for the particle recycling coefficient to approach unity when density control is lost (Brusati et al, 1992).

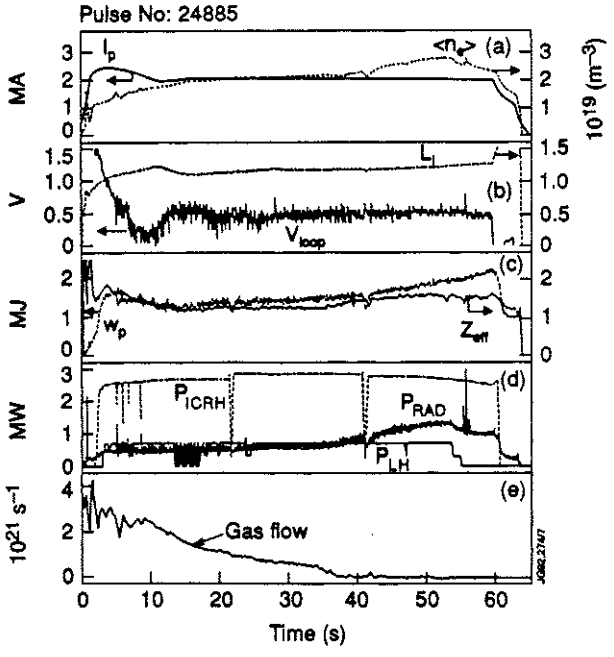

Fig 11. Plasma parameters during a one-minute pulse driven by RF at 2 MA showing the evolution of plasma particle recycling.

Volt-second saving using LHCD during the current rise of 7 MA plasmas has already been mentioned in section 2.2 (Fig 5). LHCD is well adapted to this moderate density phase where the current drive efficiency is improved by the synergistic acceleration of the LHCD fast electrons by the loop voltage necessary to raise the current. The line average density is increased to values close to 10^{20} m^{-3} during the current flat top where combined NBI/ICRH power (up to 30 MW) has been applied during 3.5 s. The total duration of the 7 MA discharge reached 8.5 s.

ICRH is well suited to high density operation since antenna-plasma coupling increases with edge density which is generally increased with the bulk density. Even more important is the predicted and observed fact that the power deposition profile is insensitive to plasma density. Fig 12 illustrates ICRH at the 20 MW level of plasmas fuelled (Schmidt et al, 1992) with a sequence of 5 deuterium pellets (size 4 mm). Heating with fast wave is seen to cope equally well with widely different density profiles which can be either peaked, flat or quite hollow.

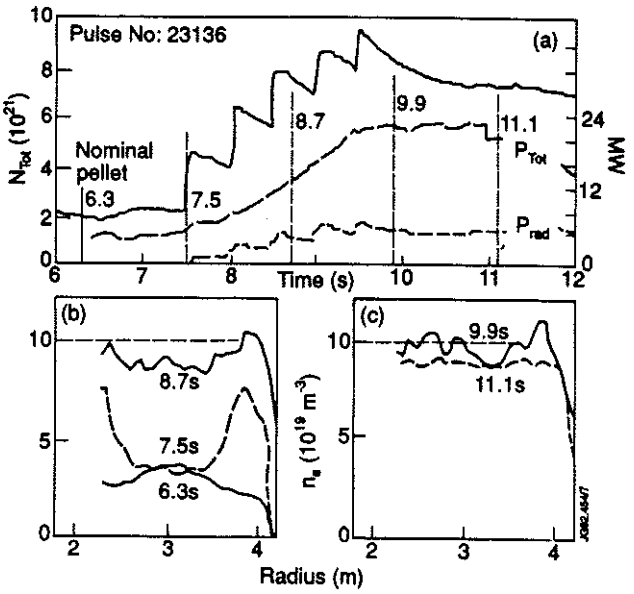

Fig 12. High power ICRH during fuelling with 4 mm pellets. The density profiles vary from parabolic to hollow, then to flat profiles without change in the ICRH efficiency.

3.4 Confinement Studies

The confinement studies reviewed in this section rely on some specific heating properties of the RF schemes. We will consider experiments taking advantage of the localised heating of ICRF or experiments based on the production of fast electrons with LHCD or of fast ions with ICRH.

3.4.1 Heat Transport with Strong On/Off Axis Heating and Current Ramp Experiments. Recent experiments have been performed in which comparisons have been made between on and off-axis ICRH following pellet injection (Balet et al, 1992). The reason for pellet injection is twofold, first to suppress the sawteeth by flattening the current profile and second to provide a heat sink in the plasma centre, such that with off-axis heating, regions of inwards heat flux can be examined. The half width of the power deposition profile is 15 cm during off-axis ICRH, a value which is small compared to the plasma radius (120 cm).

In the absence of sawteeth, the electron temperature profile responds strongly to the location of the heating (Figs 13 and 14). The data has been compared to the RLW transport model (Rebut et al, 1991) which uses a heat transport coefficient χ with a strongly non-linear function of ∇T in the expression of the heat flux $Q \sim en\,\chi\,(\nabla T - \nabla T_{crit})$. The fit of the model to the off-axis heating case, which is shown in Fig 14 is a good indication that the model has the right value of Q with ∇T at low values of ∇T of either sign. These results are in sharp contrast to other experiments in which the temperature profile is insensitive to the location of the heating profile. One key feature of the JET ICRH experiments is the lack of sawtoothing which may broaden the fast ion/electron heating profiles.

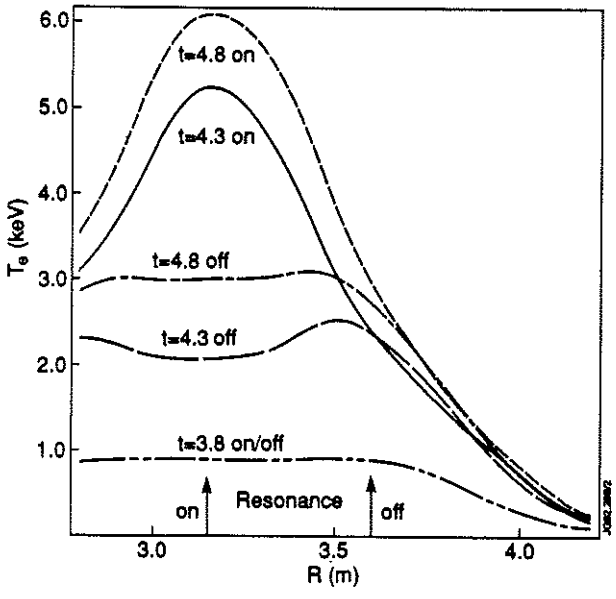

Fig 13: Evolution of T_e profiles with on/off axis ICRH after pellet injection. Inwards heat diffusion is studied in off-axis cases.

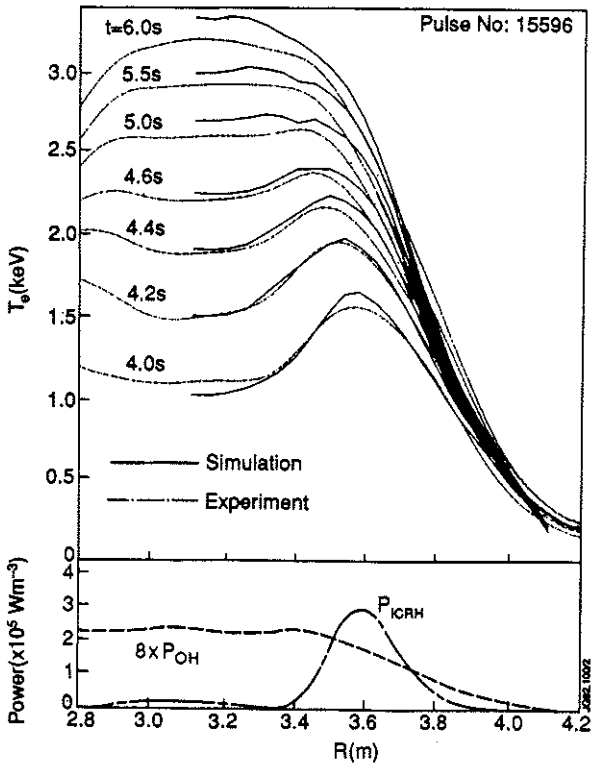

Fig 14: Comparison of the electron temperature profile evolution to a simulation based on the critical temperature gradient model (RLW). There are no sawteeth in this experiment.

Further insight on the behaviour of χ has been obtained from current ramp experiments (Challis et al, 1992) in which it is possible to decorrelate the effects of the total current I_p from those of its spatial distribution on a resistive time scale which is typically 20 times larger than the energy confinement time. ICRH is preferred in this experiment because, in the absence of core fuelling, it is easier to maintain the density constant. The results obtained from the analysis of the data are compatible with a scaling $\chi \sim B\theta^y s^\mu$ with $-2 \leq y \leq 1, -1 < \mu < 0$ where $B\theta$ is the poloidal field and s the magnetic shear. The RLW model which uses $y = -2$ and $\mu = -1$ is found again to be compatible with the results.

3.4.2 <u>Diffusion of Fast Electrons</u>. Two recent papers (Hugon et al, 1992; Gondahlekar et al, 1992) have addressed the question of the diffusion of the fast electrons created by LHCD immediately after a perturbation which was either a monster sawtooth crash or the injection of a deuterium pellet. The fast electrons are considered as markers of the magnetic configuration which can reveal the chaotic nature of the field lines inducing a diffusion process across magnetic island chains. The diffusion of the fast electrons is monitored by the non-thermal EC emission radiometer or with the beryllium, carbon or deuterium light detected at the plasma edge.

Results are compatible with a very rapid diffusion of the fast electrons for large perturbations of the poloidal field which create significant overlapping of the magnetic islands. Such fast diffusion is not present in the absence of the perturbations as it would not be compatible with the observed current drive efficiency and localisation of the fast electrons.

3.4.3 <u>Effect of Toroidal Field Ripple on Fast Ions Created by ICRH</u>. The effects of enhanced toroidal field ripple on JET plasmas have been studied (Sadler et al, 1992; Khudoleev et al, 1992) by comparing discharges with 16 TF coils to those obtained with the normal 32 coil configuration. The magnetic ripple at the limiter on the torus mid-plane $\delta = (B_{Max} - B_{Min})/(B_{Max} + B_{Min})$ increases from 1 % with 32 coils to 12.5 % with 16 coils. The enhanced ripple has unexpected detrimental effects on the quality of the H-mode. Its effect on the fast ions created by ICRH in L-mode plasmas at the first cyclotron harmonic of the hydrogen resonance is qualitatively in line with expectations for losses due to ripple well and stochastic diffusion. A high energy neutral particle analyser NPA (Petrov et al, 1992) is used to measure fast H° spectra in the 0.5 MeV to 2 MeV range. The scan of the RF resonance position performed by changing the frequency from 37 MHz to 52 MHz (Fig 15) shows that the effect of large ripple is much stronger on the low field side where the ripple is larger than on the high field side. The losses are also more severe at higher energies (Fig 16). It is not clear at this stage of the analysis that stochastic losses are as high as expected from theory.

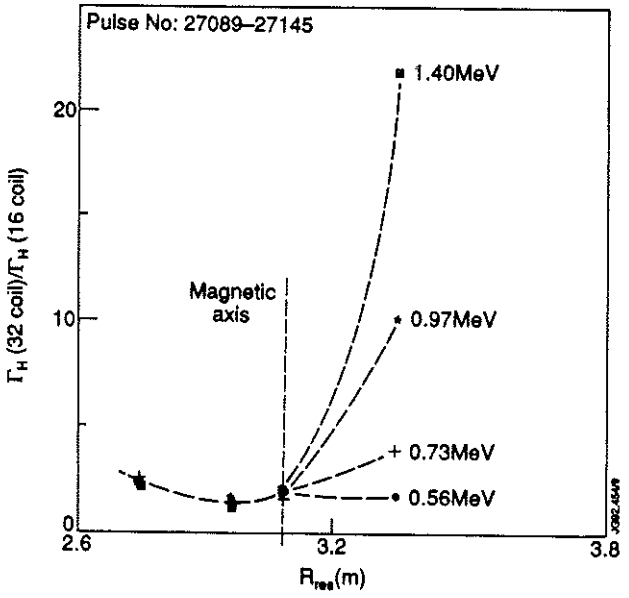

Fig 15: Flux of energetic hydrogen atoms generated by ICRH at 2 ω_{CH} during magnetic field ripple experiments with either 32 coils or 16 coils versus the position of the second harmonic resonance of hydrogen. Losses of fast ions are large on the low field side where the ripple well increases.

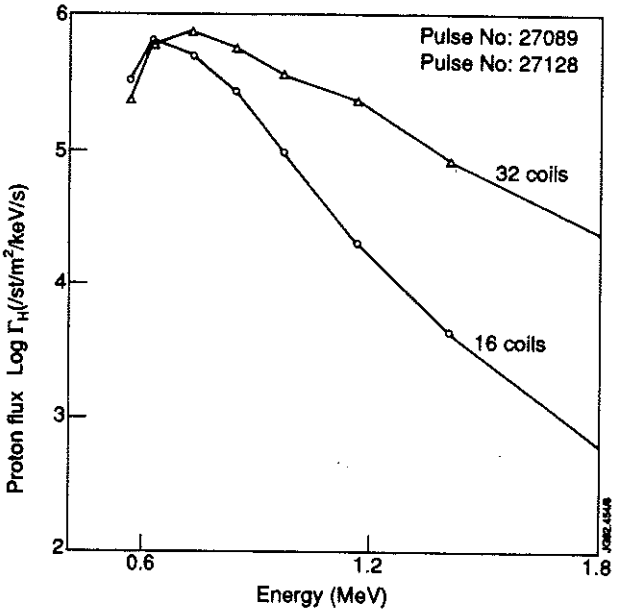

Fig 16: Energy distribution function of energetic hydrogen atoms measured by the Neutral Particle Analyser during the magnetic field ripple experiments.

4. EXPERIMENTS AND EXTRAPOLATIONS RELEVANT TO THE NEXT STEP TOKAMAK

4.1 <u>High Minority Concentration ICRH in JET and Recommended ICRH Scenarios for D/T Operation</u>

The requirement to heat a minority species at low concentration would be a constraint in a reactor. The resulting high energy tail contributes to the total plasma pressure which is limited by MHD instabilities and redistributes its energy mainly to electrons (Koch et al, 1990). It is also desirable to limit fuel dilution for optimum fusion reactivity and adding H or ^{3}He density would not be advantageous. However, one may like to keep the option of creating a high energy tail for its potential effect on plasma stability (Porcelli et al, 1992). It is therefore important to develop ICRH systems and scenarios which can

work effectively in a wide range of D/T mixtures as well as with different minority species. In this section, we substantiate the claim that a balanced D-T mixture can be heated efficiently by ICRH at $\omega = \omega_{CD}$ with low field side antennae and $k_{\|} \sim 4\ m^{-1}$.

Indeed, the size and the temperature of ITER plasmas guarantees a large single pass damping even for these unusually large concentrations so that the wave power reflected on the D/T hybrid cut-off layer is too small to generate large eigenmodes which are deleterious for antenna coupling. The scenario only applies to low field side wave launching since the $\omega = \omega_{CD}$ damping region is only accessible from the low field side, D/T hybrid resonance isolating the high field side region. The single pass absorption (SPA) contours for ITER parameters have been calculated using the ray-tracing technique. Rays are emitted from the equatorial plane on the low field side and are damped in the deuterium cyclotron resonance region by cyclotron damping, electron TTMP and electron Landau damping (note that the alpha particle damping is not included here). The minority energy used in the damping calculations is calculated from the Stix expression. An operating diagram (Fig 17) is constructed to give the damping per pass and minority energies to be expected for a given concentration and power density. The threshold for mode conversion is also represented in the diagram. If low field side antennae are used, the mode conversion which appears for $n_d/n_T > 0.1$ - 0.15 is only of concern to us when the single pass damping becomes low (say SPA < 0.5), eg when $n_D/n_T > 1$.

Similar diagrams have been drawn for JET parameters (Bhatnagar et al, 1992) showing a somewhat reduced operating range to $n_D/n_T < 0.4$ - 0.6. Note that the use of deuterium beam injection is not included here and would further increase the operating range.

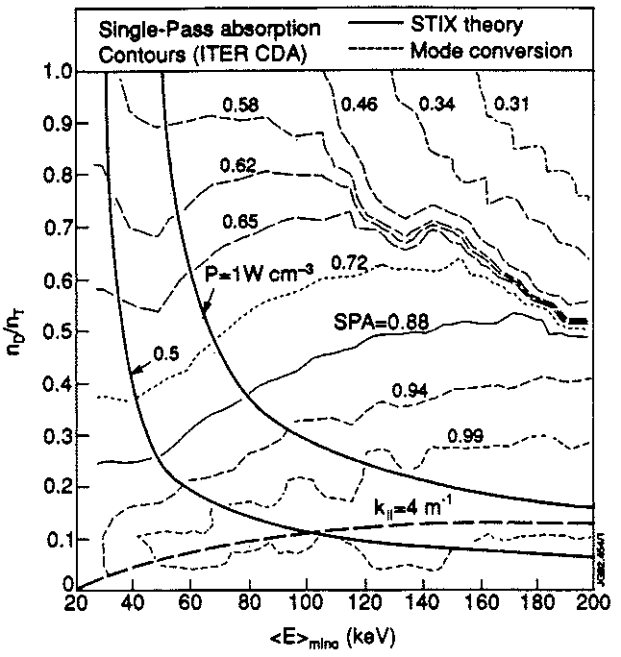

Fig 17: Single Pass Absorption contours (SPA) for the proposed ITER ICRH scenario at $\omega = \omega_{CD}$. $< E >_{mino}$ is the average deuteron energy calculated from STIX's solution for the assumed RF power density (solid lines). The mode conversion threshold is shown for $k_{//} = 4\ m^{-1}$. The size and temperature of ITER gives large SPA values even for $n_D = n_T$ and the mode conversion process becomes unimportant with low field side antennae. ($T = 15$ keV, $n_e = 9\ 10^{19}\ m^{-3}$, $k_{//} = 4\ m^{-1}$, $\nu = 36$ MHz).

It is possible to test experimentally in JET the high concentration scenario by using Hydrogen as the resonating species instead of deuterium and by replacing tritium by either deuterium or helium 3. The (H)^{3}He and the (H)D scenarios have similar SPA values than those with (D)T in ITER at similar concentration but with $k_{\|} = 7\ m^{-1}$ in JET rather than $4\ m^{-1}$ which is imposed by the larger dimensions of the antenna in ITER. The experimental results (Bhatnagar et al, 1992) are summarised in Figs 18a and 18b. The damping per pass at high concentration is inferred by the absence of eigenmodes despite being far above the mode conversion threshold. The tail energy is measured to scale as n_H^{-1} and improved ion heating is observed (Figs 18a and 18b) when the minority energy does not extend beyond the critical energy for electron drag to dominate over collisions with bulk ions. Finally the energy confinement is slightly lower in the high concentration case presumably due to the more frequent occurrence of sawteeth.

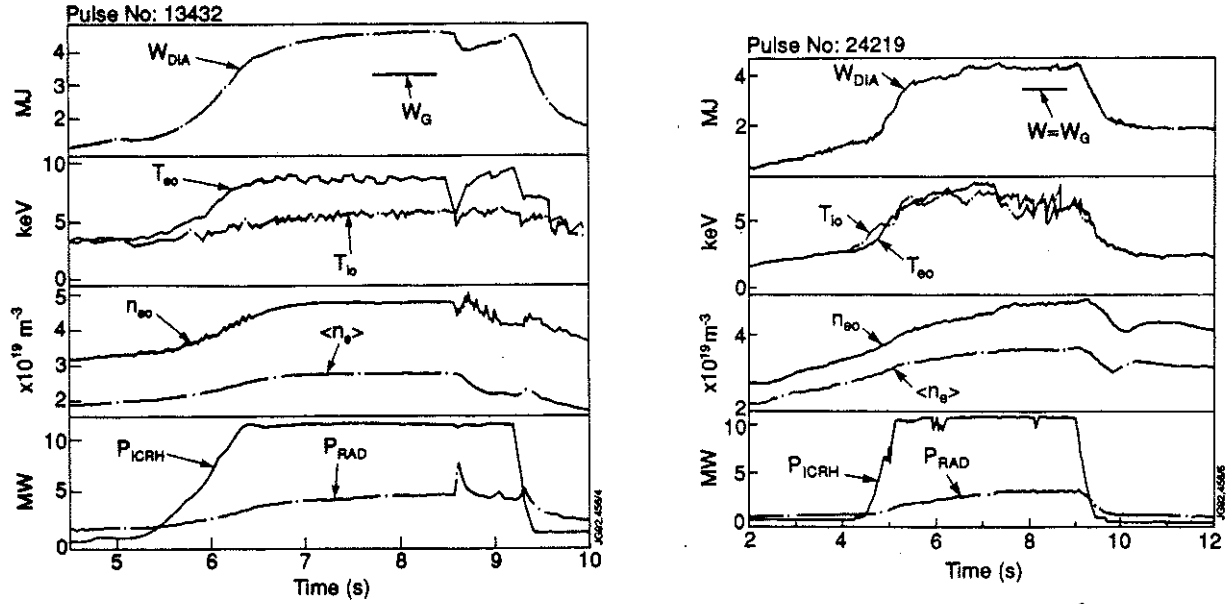

Fig 18. Evolution of the plasma parameters during ICRH of L-mode limiter plasmas in (H)^{3}He for: a) $n_H/n_{^3He} \simeq 0.06$, b) $n_H/n_{^3He} \simeq 0.63$. Ion heating is larger in the second case but sawteeth are more frequent.

4.2 Fast Wave Ion Current Drive

Ion cyclotron heating, which gives only perpendicular energy can nevertheless drive current (Fisch, 1987) with fast waves travelling preferentially in one toroidal direction due to the change in collisionality of the resonating ions which travel in phase with the preferential direction. The resonant condition $\omega - \omega_{ci} = k_{||} V_{||i}$ implies that the sign of the driven current reverses on the 2 sides of the resonance layer leading to a small net current when, as in JET, the power damped on the 2 sides are similar (note that in reactor grade plasmas the damping could be nearly one-sided). However, the effect can modify the local gradient of the plasma current density which in turn can have a strong effect on the stability of internal modes.

The minority current drive experiment was performed with ±90° phasing between the current of the 2 straps within an antenna housing. A new control system (Bosia and Jacquinot, 1991) provides automatic impedance matching whilst maintaining constant the antenna current and phase difference. Such a procedure is necessary in order to launch a well defined spectrum of travelling waves. It implies an imbalance in the forward power driving the 2 antenna straps. The wave directivity $\delta = \frac{P+ - P-}{P+ + P-}$ was $\simeq 0.3 - 0.6$ with 90°. Finally the wave frequency was chosen to locate the hydrogen cyclotron resonance around the q = 1 surface on the high field side of the torus so that local current drive effects would modify the threshold of the sawtooth instability.

The results of the experiments (Start et al, 1992) which are summarized in Fig 19 clearly show a strong effect on the sawtooth instability. The effect on the sawtooth activity is either destabilising ($\tau_{st} \simeq 0.04$ s) with -90° phasing or stabilising ($\tau_{st} \sim 1$ s) with the reverse phase. The effect is maximum for 4 MW (Fig 19). The cyclotron resonance was at R = 2.72 ± 0.05 m and the inversion radius at R = 2.80 ± 0.05 m. No effect is observed when the resonance is on-axis. Placing the resonance at the q = 1 location on the low field side produces a weaker effect and the sign of the phase for stabilisation needs to be inverted.

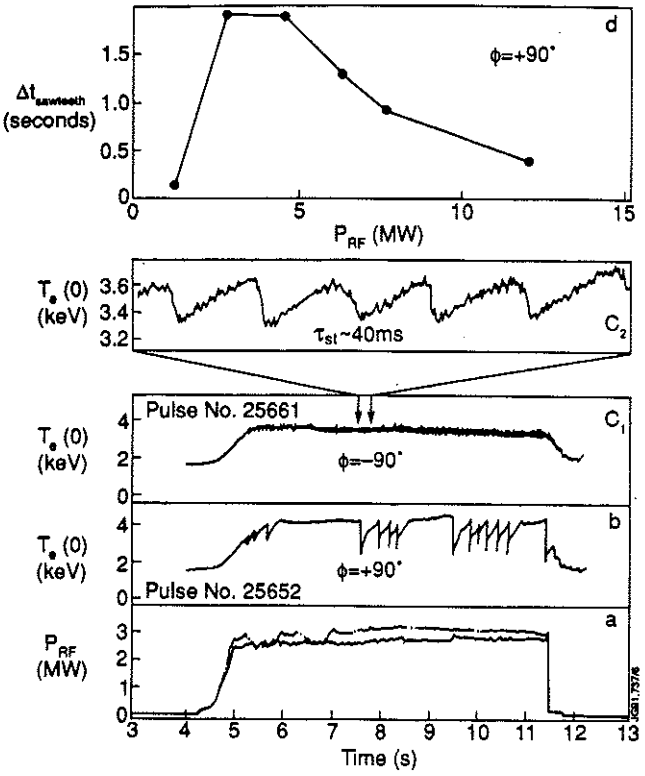

Fig 19. Ion FWCD experiments with either +90° or -90° phasing of current in the 2 antenna straps. The hydrogen cyclotron resonance is placed near the in-board q = 1 surface. Stabilisation is obtained for +90° which corresponds to decreasing the magnetic shear at q = 1 and is optimum for 3 - 4 MW.

These observations are in qualitative agreement with expectations derived from minority fast wave current drive effects. Stabilisation is predicted to result from the decrease in the shear of the poloidal field near the q = 1 surface (Porcelli et al, 1992). Fokker Planck calculations give a peak current density of 100 kAm^{-3} 10 cm away on each side of the resonance which is sufficient to reverse the current gradient at q = 1. The optimum power level and the reduction of efficiency at higher power is expected as the protons gain perpendicular energy; firstly they tend to become trapped and secondly they slow down mainly on electrons for $E > E_{crit}$. In this case the relative drift between the 2 ion species is lost. Finally, 2 physics aspects are calculated to be modified when the experiment is performed on the low field side; firstly the number of trapped minority ions increase considerably thus reducing the current drive efficiency, secondly the sign of the phase requested to produce a given change of shear is reversed. Detailed analysis of the processes are in progress.

Minority current drive and neutral beam current drive obey the same scaling: $I/P(A/W) \simeq 1.22\ 10^{19}\ J/P_d\ T_e(keV)/(n_e(m^{-3})\ RL_{og}\lambda)$ where J/P_d is dimensionless and depends on the current drive mechanism. Calculations of J/P_d for JET parameters are given in Fig 20. The efficiency is therefore expected to rise with the electron temperature. Thus the minority current drive has potential for controlling the current profile in the centre without density restrictions which affects all other methods. It should be pointed out that sawtooth control is a fast method to control the fusion burn in a tokamak. It may also be effective in controlling the accumulation of the ions resulting from the D/T burn.

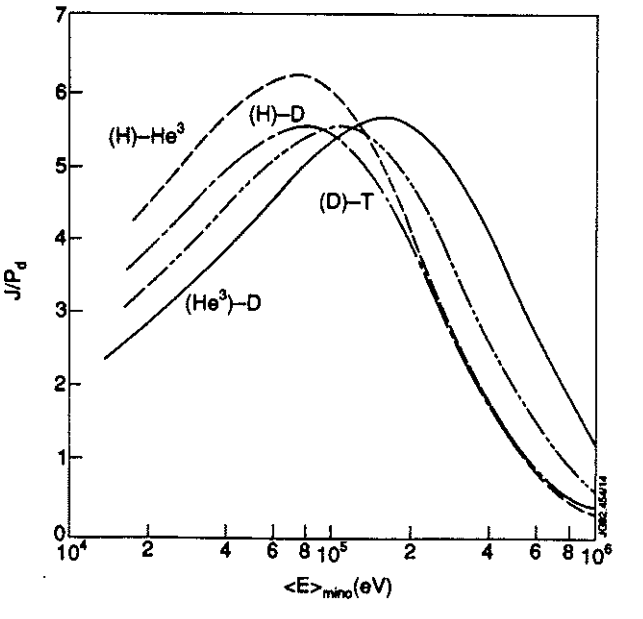

Fig 20. Normalised ion current for various resonating species and for JET plasma parameters.

We finally remark that ion current drive and electron current drive are expected to occur simultaneously for ITER

parameters as soon as significant cyclotron resonance damping exists. The 2 current drive components may either add or subtract. This remark applies to the current drive proposal at 56 MHz (Jaeger et al, 1991) for which the ion current drive resulting from the cyclotron resonance at 2 ω_{CT} has not yet been included in the calculations.

4.3 Penetration of LHCD Waves in Large Tokamaks

Lower Hybrid waves may be prevented to reach the core of large tokamak plasmas either by the accessibility condition (eg reflection at the confluence region with the fast wave) or by electron landau damping during the inward propagation. In addition, parasitic effects such as wave scattering on density fluctuations could also inhibit penetration. The large plasma size in JET offers the possibility to test the basic principles. The penetration is inferred from measurements of the Fast Electron Bremsstrahlung Emission (FEB) with 19 lines of sight in a poloidal cross section (Froissard, 1991; Peysson et al, 1992). Assuming constant emissivity of flux surfaces and using the flux geometry deduced from magnetic probe measurements, the emissivity profile is found by generalised Abel inversion of the line integrated profiles. Information is obtained in 4 energy windows ranging from 100 keV to 300 keV.

The lowest $N_{||}$ which can reach a region of density n_e (m^{-3}) and magnetic field B(T) is given for D plasmas by the approximate relation where ν is the wave frequency: $N_{||acc} \simeq 3.210^{-10}\ B^{-1}\ n_e^{0.5} + [1 + n_e\ (10^{-19}\ B^{-2} - 2.210^{-2}\nu^{-2})]^{0.5}$

The density and field dependences contained in this equation indicate that low densities and high fields allow the lower hybrid waves to penetrate deep for the low $N_{||}$ values which are required to excite the fast electrons necessary for high current drive efficiency. The JET data (Lennholm et al, 1992) is in general agreement with the accessibility equation. For instance, Fig 21 shows that the Abel inverted FEB profiles become more hollow as the central density rises from 1.5 10^{19} m^{-3} to 3.5 10^{19} m^{-3}. The peak FEB emissivity is close to the location of wave accessibility for the $N_{||}$ corresponding to the peak of the radiated spectrum. Power deposition profiles calculated with a multi pass ray tracing code including self-consistent wave damping on fast electrons (Baranov et al, 1990) provide a fair simulation of the JET data.

In summary, LH waves will penetrate beyond half radius of the JET plasma if $n_e \leq 2.5\ 10^{19}$ m^{-3}; $B_\phi \geq 3$ T and $N_{||} \geq 1.8$. Let us now address the question of the extrapolation of this result to ITER conditions. For this, we use Baranov's ray-tracing code mentioned previously assuming: $T_e = T_{eo}(1 - r^2/a^2)^3$, $n_e = n_{eo}(1 - r^2/a^2)^{0.8}$, $B_\phi = 6$ T and a launcher above the equatorial plane ($1.9 < z < 2.5$ m) with $1.825 < N_{||} < 1.975$ in order to achieve a better wave penetration.

The results of this exercise indicate that it is not useful to increase the wave frequency above 8 GHz for 2 reasons: firstly a mode conversion appears near 12 GHz preventing further penetration, secondly Landau damping becomes a dominant factor damping the wave before it reaches the confluence region. Results are summarized in Fig 22. The major conclusions are:

i) for $n_{eo} \leq 10^{20}$ m^{-3}, $T_{eo} \leq 20$ keV and $\nu = 8$ GHz the wave can penetrate near half radius. The penetration is limited by Landau damping and is nearly independent on n_e.

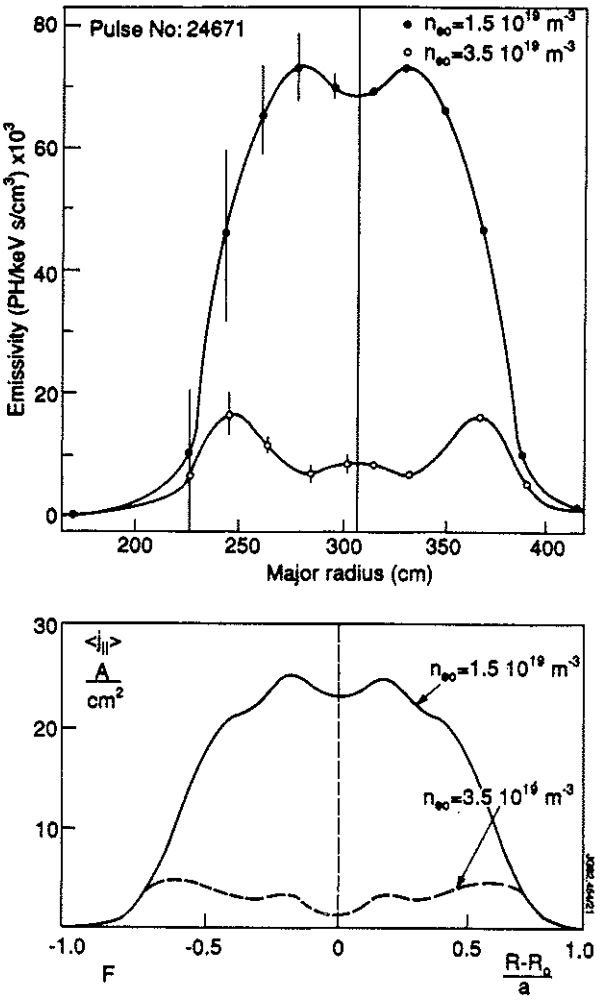

Fig 21. Radial profile of the emissivity of the fast electrons generated by LHCD and comparison to the current drive profile calculated by Baranov's ray tracing code for the parameters of the experiment.

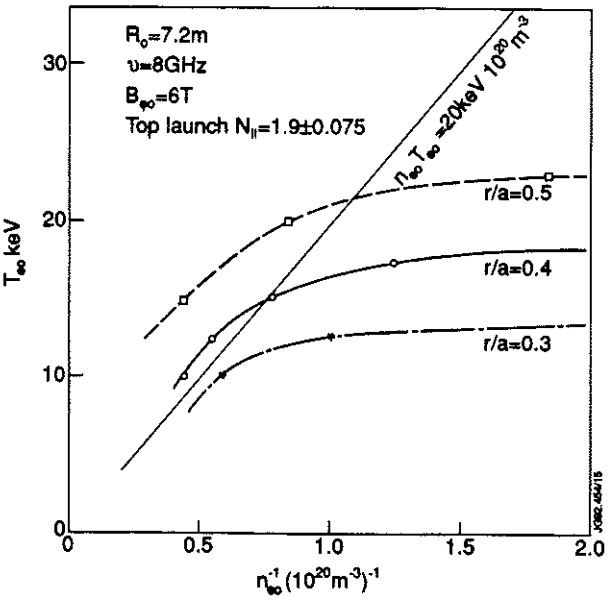

Fig 22. Contours of the penetration of LH waves predicted by Baranov's code versus n_e^{-1} for ITER size plasma. Electron Landau damping prevents increased penetration at low density.

ii) or $n_{eo} \geq 10^{20}$ m^{-3}, the accessibility becomes as in JET the limiting factor and the penetration decreases quickly when n_e increases.

Therefore LHCD appears well adapted to the current rise phase of ITER when the density and temperature are low and do not impose severe constraints on wave penetration. During the high density and high temperature burn phase, LHCD can drive current on the outer plasma region with a penetration depth which depends on the density and temperature profiles.

4.4 Full Current Drive in JET with LHCD and the Synergy with ICRH

A considerable data base has been assembled on Lower Hybrid current drive and on its performance on tokamaks. The current drive efficiency is generally measured by $\gamma = I_{CD} < n_e > R/P_d$ where I_D refers to the non-inductive current driven by the injected power P_D. γ is seen in the JT-60 tokamak (JT-60 Team, 1990) to increase with the 'peakedness' of the radiated spectrum and with the plasma electron temperature on NBI heated plasmas up to $\gamma \simeq 0.34\ 10^{20}$ m^{-2} A/W.

The maximum power injected with the JET LHCD system was 2.3 MW at $N_{||} = 1.8 \pm 0.2$. The plasma could be preheated by ICRH either in the dipole or in the monopole phasing mode. Full current drive experiments were restricted to $n_{eo} \leq 3.6\ 10^{19}$ m^{-3}. In these conditions, the LH current profile is not very different from the ohmic current profile and the discharge settles to a stationary state in about 2 s. Full current sustainment has been achieved in the following conditions (Rimini et al, 1992):

a) 0.4 MA with LHCD only in limiter plasmas
b) 2 MA for 1.5 s or 1.5 MA for 6 s with $n_{eo} = 1.6$ to $2\ 10^{19}$ m^{-3}, $P_{LHCD} = 2.2$ MW and $P_{ICRH} = 3$ to 4 MW in limiter plasmas.
c) 1 MA for 4 s in double null elmy H-mode plasmas with $n_{eo} = 3.6\ 10^{19}$ m^{-3}, $P_{LHCD} = 1.5$ MW, $P_{ICRH} = 3$ MW. In this last condition, the contribution of the neo-classical bootstrap current was much larger than the previous cases and would amount to 40 % of the plasma current.

The current drive efficiency γ has been estimated in 2 ways. Firstly we consider an engineering efficiency $\gamma_{eng} = I_{NI} < n_e > R/P_{in}$ where I_{NI} is the total non-inductive current including the bootstrap contribution and $P_{in} = P_{LHCD} + P_{ICRH}$. The maximum value of γ_{eng} reached $0.25\ 10^{20}$ m^{-2} A/W (Fig 23a). Secondly, we consider a "physics" efficiency $\gamma_{phys} = (I_{NI} - I_{Bs}) < n_e > R/(P_{LHCD} + P_{syn})$ where the bootstrap contribution is estimated from the measurement of β_p and P_{syn} is the part of the ICRH power which is transferred by synergy to the fast electrons created by LHCD; this term contributes to the current drive even when the ICRH antennae are not phased to launch a travelling wave as in this experiment. P_{syn} is determined from the measurement of the direct electron heating source P_e with LH power modulation experiment: $P_{syn} = P_e - 0.8\ P_{LH}$. The factor 0.8 results from the power balance in experiments with LH alone. γ_{phys} can reach maximum values of $0.45\ 10^{20}$ m^{-2} A/W and is found to increase linearly with $\overline{n} < T_e >$ (Fig 23b). Note that P_{syn} can be as large as 40 % of the LH power but never exceeded 18 % of the ICRH power.

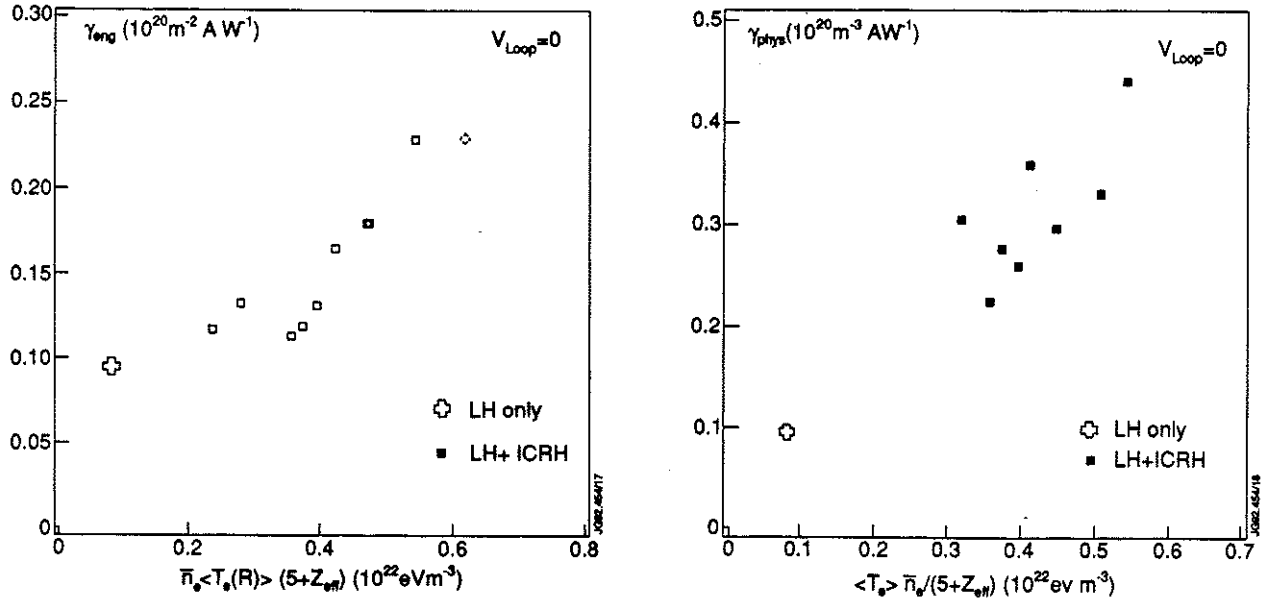

Figs 23a and b: Current drive efficiency for zero loop voltage experiments in JET. a) Engineering efficiency $\gamma_{eng} = < n_e > R\, I_{NI}/(P_{ICRH} + P_{LH})$. b) Physics efficiency $\gamma_{phys} = < n_e > R(I_{NI} - I_{BS})/(P_{LH} + P_{SYN})$. The definition of γ_{phys} isolates the current drive contribution due to fast electrons. The "ultimate" γ_{phys} value for relativistic electrons cannot exceed = $2\ 10^{20}$ m^{-2} AW^{-1}.

The synergy with ICRH was first discovered experimentally in JET by noting that the FEB intensity and photon temperature can considerably exceed values with LH only revealing acceleration of electrons to energies several times larger than the highest energy corresponding to the $n_{||}$ spectrum of the launched LH waves (~ 100 keV). The effect is unchanged when the loop voltage drops to zero (Gormezano et al, 1991). This analysis has been extended (Brusati et al, 1992) by combining the

information from the non-thermal electron cyclotron emission spectrum which is sensitive to the perpendicular energy of the fast electrons to the information originating from the FEB camera which provides measurements of the fast electron localisation and of the parallel energy of the fast electrons. The analysis assumes that the fast electron distribution function can be represented by anisotropic tri-maxwellian determined by $T_{\|f}$, $T_\perp$ and $T_{\|b}$ where the indices f and b stand for "forward" and "backward" respectively. It is found that $T_{\|f} = 120$ keV, $T_\perp = 25$ keV with LH only and $T_{\|f} = 800$ keV, $T_\perp = 80$ keV in the strongest synergistic case ($P_{LH} = 2$ MW, $P_{ICRH} = 3$ MW).

The physics of the synergy is unclear. Direct absorption of the fast wave on the fast electron population is insufficient to provide the observed energy transfer (Cox et al, 1991). Let us now consider the possibility of mode conversion at the ion-ion hybrid resonance to an ion Bernstein wave (Jacquinot, 1985) which is damped on the fast electron. The fraction of the power converted at each pass can be estimated using Budden's solutions for a wave launched from the low field side:

$$\Delta P/P = e^{-x} - e^{-2x} \text{ with } x = \pi \Delta R_e k_\perp$$

where ΔR_e is the distance between the cut-off and the hybrid resonance ($\Delta R_e = 0.25\ R_o\ n_H/n_D$) and $k_\perp$ is the transverse wave number away from the singular layer. $\Delta P/P$ has a broad maximum of 0.25 for $x = 0.69$ which corresponds to $n_H/n_D \sim 1.5\ 10^{-2}$ for the conditions of the experiments ($k_\perp = 22\ m^{-1}$) (NB: including hot plasma effects will increase this value). This proposal would be compatible with the observations that the synergy appears only with monopole phasing (low $k_\|$ values are required for mode conversion) and passes through a maximum as a function of P_{ICRH} (mode conversion is quenched when the minority ion energy is too large). We note that the mode conversion mechanism would reach nearly 100 % with high field antenna launch without the constraint of an optimum concentration. It is therefore conceivable that the synergy could be used in balanced D/T mixture with a high field side launch. The RF current would be localised near the D/T ion hybrid layer. On the contrary, if low field side antennae are used, the scaling of x with R is not favourable as the optimum concentration which decreases with R and n_e would become very small.

4.5 The Prospect of a Steady State Fusion Reactor

In a steady state fusion reactor, the full current should be driven by a combination of 2 non-inductive current sources: the first one is free and comes from the bootstrap current given by $\alpha_{BS} = I_{BS}/I_p = \beta_p/A^{1/2}$ where $A = R/a$. The second one comes from an external auxiliary source P_{CD} and requires to recirculate some of the power generated by the fusion reactor. Let $P_{CD} = \gamma_r P_{fus}$. A value of $\gamma_r = 0.04$ would correspond to recycling about 20 % of the generated electrical power when the cascade of efficiencies are taken into account. We therefore require a current drive efficiency:

$$\gamma = \frac{< n > R\ I(1 - \alpha_{BS})}{\gamma_r\ P_{fus}} \tag{1}$$

Let us now assume that the fusion power is beta limited: $\beta_t \sim g I_p/aB$. Replacing in equation 1 gives us:

$$\gamma \sim \frac{< n > (1 - \alpha_{BS})}{\gamma_r\ g^2\ I\ B^2\ k} \tag{2}$$

where k is the elongation and g the Troyon factor (typically $g \sim 2.8$).

We now need to express that the current appearing in equation 2 is the value required to achieve ignition. This is done with the assumption that the energy confinement time is given by the Goldston regression formula with a multiplicator γ_g:

$$\tau = \gamma_g\ \tau_g = 3.7\ 10^{-2}\ \gamma_g I_p\ P^{-0.5}\ R^{1.38}\ (R/a)^{0.37}\ k^{1/2} \tag{3}$$

It should be borne in mind at this point that the increase of τ with R/a is not documented with a sufficient data base and is somewhat controversial as τ is predicted to increase when the plasma radius is decreased with the other parameters kept constant. Using profile factors and dilution factors generally assumed for ignited plasmas (Bickerton, 1989) and for ITER (Tomabechi, 1991), we find (SI units unless stated):

$$I(MA) = 122\ R^{0.12}\ \gamma_g^{-1}\ A^{-1.37} \tag{4}$$

$$\alpha_{BS} = 5.4\ 10^{-3}\ \gamma_g\ k\ g\ A^{1.87}\ B\ R^{-1.12} \tag{5}$$

$$P_{fus}\ (MW) = 19.5\ g^2 B^2 R^{1.24} k\ \gamma_g^{-2}\ A^{-2.74} \tag{6}$$

Combining these equations yields the minimum current drive efficiency to sustain the current without excessive power consumption:

$$\gamma = 6.24 \frac{\gamma_g}{\gamma_r}\ \frac{< n > A^{1.37}}{R^{0.12}\ g^2\ B^2\ k}\ (1 - \alpha_{BS}) \tag{7}$$

This expression stresses the importance of working at high field and low density in order to minimise the required efficiency. Operation at beta limit gives:

$$< n\,T > = 0.124 \frac{g\,I\,AB}{R} \quad (10^{20}\ m^{-3},\ keV,\ MA) \tag{8}$$

and with a Goldston type regression formula:

$$< n\,T > = 15.1 \frac{gB}{\gamma_g\, R^{0.88}\, A^{0.37}} \quad (10^{20}\ m^{-3},\ keV,\ MA) \tag{9}$$

Combining equations (9) and (7), the minimum current drive efficiency is given by:

$$\gamma = \frac{94.2}{\gamma_r} \frac{A}{< T > RgBk} (1 - \alpha_{BS}) \tag{10}$$

It has been shown that operation at low temperature reduces accumulation of helium in the plasma core (Bickerton, 1992). Fig 25 has been done with : $< T > = 15$ keV, $k = 1.8$, $\gamma_g = 1.5$ and $q = 3.1$, where q_ψ is the Shafranov q at the plasma edge:

$$q_\psi = \frac{5\,RB}{A^2 I} \left[\frac{1 + k^2}{2}\right] \left[1 - \frac{1}{A^2}\right]^{-2}$$

which are values presently being considered for ITER. It is clear that the best current drive efficiencies obtained in today's experiments are not sufficient to operate a reactor at the large densities which are thought to be required to limit the thermal loading of the divertor. The only practical solution would be, as proposed previously in the SSTR proposal (Seki et al, 1990), to let the bootstrap current do most of the current drive by working at high field, high aspect ratio. The SSTR proposal found, in agreement with equation 7, that $\gamma = 0.5\ 10^{20}$ would be adequate at high field (9 T), high aspect ratio ($A = 4.1$) and high Troyon parameter ($g = 3.3$). The controversial aspect is that large A is obtained by reducing the plasma radius and consequently reducing the plasma current to 12 MA. There is not a sufficient data base with large tokamaks to choose this regime for ITER but new experiments should aim at this promising land.

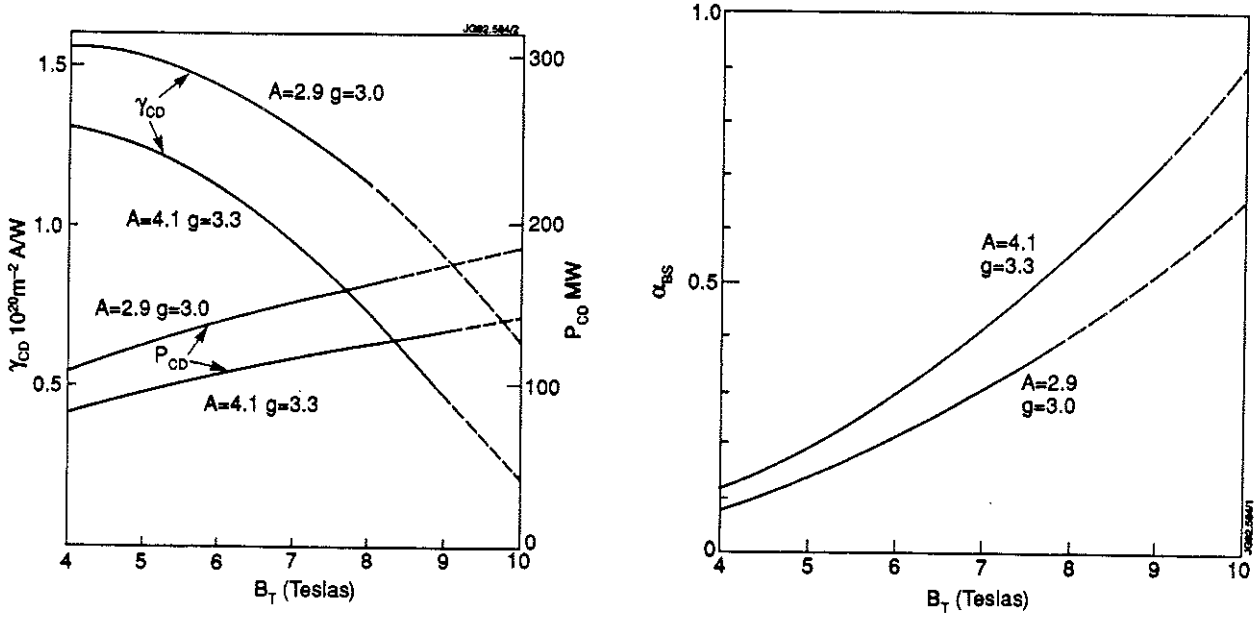

Figs 24a and b: Current drive efficiency γ_{CD} required to sustain the full current in an ignited reactor with $< T > = 15$ keV and $q_\psi = 3.1$. Dotted points correspond to magnetic field values at the coil in excess of 15 T. The power of the auxilliary current drive system is limited to 0.04 P_{fusion} or 20 % of the electrical power output. The bootstrap fraction is calculated with the same hypotheses.

Finally we note that the prospect to increase γ above the best value obtained experimentally is limited to $\gamma \sim 10^{20}\ m^{-2}\ AW^{-1}$ when the current carrying electrons reach a tail temperature around 1 MeV which corresponds to the minimum power necessary to maintain against synchrotron radiation and collisions with the plasma. If no high energy tail is formed as expected in pure fast wave current drive then γ is limited to a value of 0.2 to 0.3 10^{20} (Fig 25) for the parameters corresponding to the ITER -CDA ($T_{eo} = 33$ keV, $n_{eo} = 1.1\ 10^{20}\ m^{-3}$ $B = 4.85$ T).

5. CONCLUSIONS

In this article we have reviewed the latest developments of the 2 large RF systems installed on the JET device. We have emphasised the versatility and availability aspects. Feedback systems alleviate to a large extent the traditional difficulties of plasma-antenna coupling. Consequently these systems have been used as regular tools in a wide ranging programme covering major aspects on high plasma performance, basic confinement problems and specific wave issues relevant to the next generation of tokamaks.

ICRH appears as a prime candidate for heating large tokamaks since a narrow power deposition profile can be localised at will in the tokamak independently of the plasma density and of the plasma size. We have shown that the constraint of heating a minority species can be removed for plasma size and temperature similar to or exceeding the JET parameters because the wave is damped at the cyclotron resonance before reaching the ion-ion hybrid mode conversion layer. Heating a D/T mixture with $0.25 < n_D/n_T \leq 1.2$ at $\omega = \omega_{CD}$ near the axis is proposed as a basic ITER heating scenario which optimises ion heating en-route to ignition (Koch et al, 1990). This corresponds to the centre of the frequency band $17 \leq \nu \leq 66$ MHz which has been proposed (Jacquinot, Bures and the JET Team, 1992) to operate both in current drive and in several ion resonance regimes giving a large domain of possible operation scenarios.

LHCD appears as a prime tool for current drive for its ability to generate fast electrons and currents for the highest efficiency recorded so far. The penetration of LH waves in large hot plasmas was found to be in general agreement with calculated accessibility boundaries. For ITER parameters at ignition, LH waves will not penetrate beyond half the plasma radius. LHCD is well adapted to save volt-seconds during the current rise where the density is moderate and the inductive electric field contributes to the acceleration of the fast electrons. Synergy with ICRH has been observed to accelerate fast electrons near the MeV range and efficient full wave current drive experiments have been performed. There is clearly a route towards the high efficiencies required in a reactor but the physics mechanisms are unclear and will require further studies.

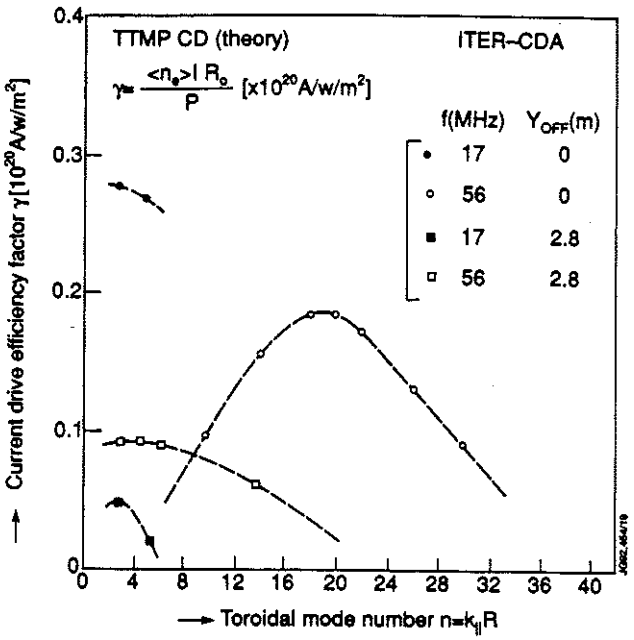

Fig 25: Current drive efficiency by FWCD in the 17 and the 56 MHz regimes. Calculations for ITER-CDA parameters without any electron tail formation. Y_{off} refers to the antenna position with respect to the equatorial plane.

A steady state fusion reactor operating at high density with the standard aspect ratio has been shown to require current drive efficiencies which are beyond the present state of art. We nevertheless propose to pursue actively the research in this field of current drive in order to contribute to critical issues relevant to the next tokamaks such as burn control via the sawtooth instability as in the experiments reported here or even full current drive if it can be shown that bootstrap dominated discharges at large aspect ratio possess the required confinement properties to achieve ignition in an economical way.

ACKNOWLEDGEMENT

It is a pleasure to acknowledge the contributions of CEA (Cadarache) in the construction of one of the 2 prototype LHCD launchers and also Dr G Rey in the operation of the system. The work has also benefited from collaborations with AEA, ERM/KMS and CEA on current drive modelling. Some recent developments on matching with phased FWCD antenna have been made jointly with the Oak Ridge National Laboratory. Pellet injection results were obtained under a collaboration agreement between the JET Joint Undertaking and the US Department of Energy.

REFERENCES

Balet, B., D. Boucher, J. G. Cordey et al, 19th EPS Conf. Innsbruck, 1992, Vol. 16C, part 1, p. 59.
Baranov, Y., A. R. Esterkin, A. D. Piliya, JET-P Letters Vol. 51, N12, 1990, p. 150
Bhatnagar, V. P., J. Jacquinot and D. F. H. Start, IAEA Tech. Comm. Meeting on FWCD in Reactor Scale Tokamaks, Arles, 1991, p. 110.
Bhatnagar, V. P. et al, Europhys. Top. Conf. on RF Heating and Current Drive of Fus. Devices, Brussels, 1992, Vol. 16E, p. 105.
Bickerton, R. J., Physics Scaling of Reactor Plasmas, Fus. Research Center report 335, Austin, Texas (1989).
Bickerton, R. J. (1992). Dynamics of a Steady State D-T Buring Tokamak Plasma, JET-R(92)03.
Bosia, G. and J. Jacquinot, IAEA Tech. Comm. Meeting on FWCD in Reactor Scale Tokamaks, Arles, 1991, p. 471.
Brusati, M., M. Bures et al, 19th EPS Conf. Innsbruck, 1992, Vol. 16C, part 1, p. 37.
Brusati, M. et al, Europhys. Top. Conf. on RF Heating and Current Drive of Fus. Devices, Brussels, 1992, Vol. 16E, p. 225.
Bures, M., J. Jacquinot, R. Lawson et al (1991). In: Plasma Phys. and Contr. Fus., Vol. 33, 937.
Bures, M. et al, 19th EPS Conf. Innsbruck, 1992, Vol. 16C, part 2, p. 881.
Challis, C. D. et al, JET-P(92)15, submitted to Nucl. Fus.
Challis, C. D. et al, Europhys. Top. Conf. on RF Heating and Current Drive of Fus. Devices, Brussels, 1992, Vol. 16E, p. 109.
Cordey, J. G. (1988). In: Plasma Phys. and Contr. Fus., 30, 1625.
Cox, M., M. R. O'Brien, C. D. Warrick, IAEA Tech. Comm. Meeting on FWCD in Reactor Scale Tokamaks, Arles, 1991, p. 122.
D'Ippolito, D., J. Myra, M. Bures, J. Jacquinot (1991). In: Bull. Am. Phys. Soc. II, Vol. 36, p. 2341.

Ekedahl, A. et al, Europhys. Top. Conf. on RF Heating and Current Drive of Fus. Devices, Brussels, 1992, Vol. 16E, p. 221.
Eriksson, L., private communication.
Fisch, N. (1987). Review of Modern Phys., Vol. 59, p. 175.
Froissard, P. et al (1991). Proc. 18th EPS Conf., Berlin, Vol. 15C, part 3, p. 389.
Gondhalekar, A. et al, 19th EPS Conf., Innsbruck, 1992, Vol. 16C, part 1, p. 147.
Gormezano, C. et al (1987). Proc. 12th Symp. Fus. Eng., Monterrey, Vol. 1, p. 38
Gormezano, C., IAEA Tech. Comm. Meeting on FWCD in Reactor Scale Tokamaks, Arles, 1991, p. 244.
Hender, T. C. et al, 19th EPS Conf., Innsbruck, 1992, Vol. 16C, part 1, p. 335.
Hugon, M. et al (1992). In: Nucl. Fus., Vol. 32, p. 33 .
Hugon, M. et al, 19th EPS Conf., Innsbruck, 1992, Vol. 16C, part 1, p. 119.
Jacquinot, J. and G. Sadler (1992). In: Fus. Tech. special issue on D-^{3}He Fus., Vol. 21, p. 2254.
Jacquinot, J. and the JET Team (1991). In: Plasma Phys. and Contr. Fus., Vol. 13, p. 1657
Jacquinot, J., M. Bures and the JET Team (1992). Accepted for publication in Phys. Fluids .
Jaeger, F. and D. Bachelor, IAEA Tech. Comm. Meeting on FWCD in Reactor Scale Tokamaks, Arles, 1991, p. 86.
The JET Team (1991). In: Plasma Phys. and Contr. Fus., IAEA, Vol. 1, p. 27 .
The JT-60 Team (1990). In: Plasma Phys. and Contr. Fus., IAEA, Vol. 1, p. 53.
Kaye, A. et al, invited paper at this conf. submitted to Plasma Phys. and Contr. Fus.
Keilhacker, M. and the JET Team (1991). In: Plasma Phys. and Contr. Fus., Vol. 13, p. 1453
Khudoleev A. V. et al, 19th EPS Conf., Innsbruck, 1992, Vol. 16C, part 1, p. 151, also in this conf.
Kikuchi M. (1990). Nucl. Fus. 30, 2, 265.
Koch, R., D. Van Eester, V. Nys (1990). In: Plasma Phys. and Contr. Fus., IAEA, Vol. 3, p. 605.
Lennholm, M., et al, Europhys. Top. Conf. on RF Heating and Current Drive of Fus. Devices, Brussels, 1992, Vol. 16E, p. 269.
Petrov, M., P., 19th EPS Conf., Innsbruck, 1992, Vol. 16C, part 2, p. 1031.
Peysson, Y. et al (1992). Europhys. Top. Conf. on RF Heating and Current Drive of Fus. Devices, Brussels, Vol. 16E, p. 217
Rebut, P. H. (1992). Report JET-P(92)21, JET Joint Undertaking, Abingdon, Oxon (UK).
Rebut, P. H., M. Watkins, D. Gambier and D. Boucher (1991). In: Phys. Fluids, B3 (8) 2209 .
Righi, E. et al, Europhys. Top. Conf. on RF Heating and Current Drive of Fus. Devices, Brussels, 1992, Vol. 16E, p. 113.
Rimini, F. et al, Europhys. Top. Conf. on RF Heating and Current Drive of Fus. Devices, Brussels, 1992, Vol. 16E, p 229.
Sadler, G., 19th EPS Conf., Innsbruck, 1992, Vol. 16C, part 1, p. 167.
Schmidt, G. and the JET Team (1989). In: Plasma Phys. and Contr. Fus., IAEA Conf. on Plasma Phys. and Contr. Fus., Nice, 1988, Vol. 1, p. 215 .
Schmidt, G. et al, 19th EPS Conf., Innsbruck, 1992, Vol. 16C, part 1, p. 255.
Seki, Y., M. Kikuchi, et al (1990). IAEA Conf. on Plasma Phys. and Contr. Fus., Washington DC, IAEA-CN-53/G-1-2.
Start, D. et al, 19th EPS Conf., Innsbruck, 1992, Vol. 16C, part 2, p. 897.
Tomabechi, K., J. P. Gilleland, Y. A. Sokolov, R. Toschi, and ITER Team (1991). In: Nucl. Fus. Vol. 31, 1135.
Tomabechi et al (1991). In: Nucl. Fus. Vol. 31, 6, 1135.
Tonon, G. and Equipe Tore Supra, invited paper, 14th Symp. on Fus. Tech., San Diego, 1991.
Tubbing, B. et al (1991). In: Nucl. Fus., Vol. 31, p. 389.

Appendix I

THE JET TEAM

JET Joint Undertaking, Abingdon, Oxon, OX14 3EA, U.K.

J.M. Adams[1], B. Alper, H. Altmann, A. Andersen[14], P. Andrew, S.Ali-Arshad, W. Bailey, B. Balet, P. Barabaschi, Y. Baranov, P. Barker, R. Barnsley[2], M. Baronian, D.V. Bartlett, A.C. Bell, G. Benali, P. Bertoldi, E. Bertolini, V. Bhatnagar, A.J. Bickley, D. Bond, T. Bonicelli, S.J. Booth, G. Bosia, M. Botman, D. Boucher, P. Boucquey, M. Brandon, P. Breger, H. Brelen, W.J. Brewerton, H. Brinkschulte, T. Brown, M. Brusati, T. Budd, M. Bures, P. Burton, T. Businaro, P. Butcher, H. Buttgereit, C. Caldwell-Nichols, D.J. Campbell, D. Campling, P. Card, G. Celentano, C.D. Challis, A.V.Chankin[23], A. Cherubini, D. Chiron, J. Christiansen, P. Chuilon, R. Claesen, S. Clement, E. Clipsham, J.P. Coad, I.H. Coffey[24], A. Colton, M. Comiskey[4], S. Conroy, M. Cooke, S. Cooper, J.G. Cordey, W. Core, G. Corrigan, S. Corti, A.E. Costley, G. Cottrell, M. Cox[7], P. Crawley, O. Da Costa, N. Davies, S.J. Davies[7], H. de Blank, H. de Esch, L. de Kock, E. Deksnis, N. Deliyanakus, G.B. Denne-Hinnov, G. Deschamps, W.J. Dickson[19], K.J. Dietz, A. Dines, S.L. Dmitrenko, M. Dmitrieva[25], J. Dobbing, N. Dolgetta, S.E. Dorling, P.G. Doyle, D.F. Düchs, H. Duquenoy, A. Edwards, J. Ehrenberg, A. Ekedahl, T. Elevant[11], S.K. Erents[7], L.G. Eriksson, H. Fajemirokun[12], H. Falter, J. Freiling[15], C. Froger, P. Froissard, K. Fullard, M. Gadeberg, A. Galetsas, L. Galbiati, D. Gambier, M. Garribba, P. Gaze, R. Giannella, A. Gibson, R.D. Gill, A. Girard, A. Gondhalekar, D. Goodall[7], C. Gormezano, N.A. Gottardi, C. Gowers, B.J. Green, R. Haange, A. Haigh, C.J. Hancock, P.J. Harbour, N.C. Hawkes[7], N.P. Hawkes[1], P. Haynes[7], J.L. Hemmerich, T. Hender[7], J. Hoekzema, L. Horton, J. How, P.J. Howarth[5], M. Huart, T.P. Hughes[4], M. Huguet, F. Hurd, K. Ida[18], B. Ingram, M. Irving, J. Jacquinot, H. Jaeckel, J.F. Jaeger, G. Janeschitz, Z. Jankowicz[22], O.N. Jarvis, F. Jensen, E.M. Jones, L.P.D.F. Jones, T.T.C. Jones, J-F. Junger, F. Junique, A. Kaye, B.E. Keen, M. Keilhacker, W. Kerner, N.J. Kidd, R. Konig, A. Konstantellos, P. Kupschus, R. Lässer, J.R. Last, B. Laundy, L. Lauro-Taroni, K. Lawson[7], M. Lennholm, J.Lingertat[13], R.N. Litunovski, A. Loarte, R. Lobel, P. Lomas, M. Loughlin, C. Lowry, A.C. Maas[15], B. Macklin, C.F. Maggi[16], G. Magyar, V. Marchese, F. Marcus, J. Mart, D. Martin, E. Martin, R. Martin-Solis[8], P. Massmann, G. Matthews, H. McBryan, G. McCracken[7], P. Meriguet, P. Miele, S.F. Mills, P. Millward, E. Minardi[16], R. Mohanti[17], P.L. Mondino, A. Montvai[3], P. Morgan, H. Morsi, G. Murphy, F. Nave[27], S. Neudatchin[23], G. Newbert, M. Newman, P. Nielsen, P. Noll, W. Obert, D. O'Brien, J. O'Rourke, R. Ostrom, M. Ottaviani, S. Papastergiou, D. Pasini, B. Patel, A. Peacock, N. Peacock[7], R.J.M. Pearce, D. Pearson[12], J.F. Peng[26], R. Pepe de Silva, G. Perinic, C. Perry, M.A. Pick, J. Plancoulaine, J-P. Poffé, R. Pohlchen, F. Porcelli, L. Porte[19], R. Prentice, S. Puppin, S. Putvinskii[23], G. Radford[9], T. Raimondi, M.C. Ramos de Andrade, M. Rapisarda[29], P-H. Rebut, R. Reichle, S. Richards, E. Righi, F. Rimini, A. Rolfe, R.T. Ross, L. Rossi, R. Russ, H.C. Sack, G. Sadler, G. Saibene, J.L. Salanave, G. Sanazzaro, A. Santagiustina, R. Sartori, C. Sborchia, P. Schild, M. Schmid, G. Schmidt[6], H. Schroepf, B. Schunke, S.M. Scott, A. Sibley, R. Simonini, A.C.C. Sips, P. Smeulders, R. Smith, M. Stamp, P. Stangeby[20], D.F. Start, C.A. Steed, D. Stork, P.E. Stott, P. Stubberfield, D. Summers, H. Summers[19], L. Svensson, J.A. Tagle[21], A. Tanga, A. Taroni, C. Terella, A. Tesini, P.R. Thomas, E. Thompson, K. Thomsen, P. Trevalion, B. Tubbing, F. Tibone, H. van der Beken, G. Vlases, M. von Hellermann, T. Wade, C. Walker, D. Ward, M.L. Watkins, M.J. Watson, S. Weber[10], J. Wesson, T.J. Wijnands, J. Wilks, D. Wilson, T. Winkel, R. Wolf, D. Wong, C. Woodward, M. Wykes, I.D. Young, L. Zannelli, A. Zolfaghari[28], G. Zullo, W. Zwingmann.

PERMANENT ADDRESSES

1. UKAEA, Harwell, Didcot, Oxon, UK.
2. University of Leicester, Leicester, UK.
3. Central Research Institute for Physics, Budapest, Hungary.
4. University of Essex, Colchester, UK.
5. University of Birmingham, Birmingham, UK.
6. Princeton Plasma Physics Laboratory, New Jersey, USA.
7. UKAEA Culham Laboratory, Abingdon, Oxon, UK.
8. Universidad Complutense de Madrid, Spain.
9. Institute of Mathematics, University of Oxford, UK.
10. Freien Universität, Berlin, F.R.G.
11. Royal Institute of Technology, Stockholm, Sweden.
12. Imperial College, University of London, UK.
13. Max Planck Institut für Plasmaphysik, Garching, FRG.
14. Risø National Laboratory, Denmark.
15. FOM Instituut voor Plasmafysica, Nieuwegein, The Netherlands.
16. Dipartimento di Fisica, University of Milan, Milano, Italy.
17. North Carolina State University, Raleigh, NC, USA
18. National Institute for Fusion Science, Nagoya, Japan.
19. University of Strathclyde, 107 Rottenrow, Glasgow, UK.
20. Institute for Aerospace Studies, University of Toronto, Ontario, Canada.
21. CIEMAT, Madrid, Spain.
22. Institute for Nuclear Studies, Otwock-Swierk, Poland.
23. Kurchatov Institute of Atomic Energy, Moscow, USSR
24. Queens University, Belfast, UK.
25. Keldysh Institute of Applied Mathematics, Moscow, USSR.
26. Institute of Plasma Physics, Academica Sinica, Hefei, P. R. China.
27. LNETI, Savacem, Portugal.
28. Plasma Fusion Center, M.I.T., Boston, USA.
29. ENEA, Frascati, Italy.

At 1st July, 1992